iScience

CellPress
OPEN ACCESS

Article

Thymus antibody-secreting cells possess an interferon gene signature and are preferentially expanded in young female mice

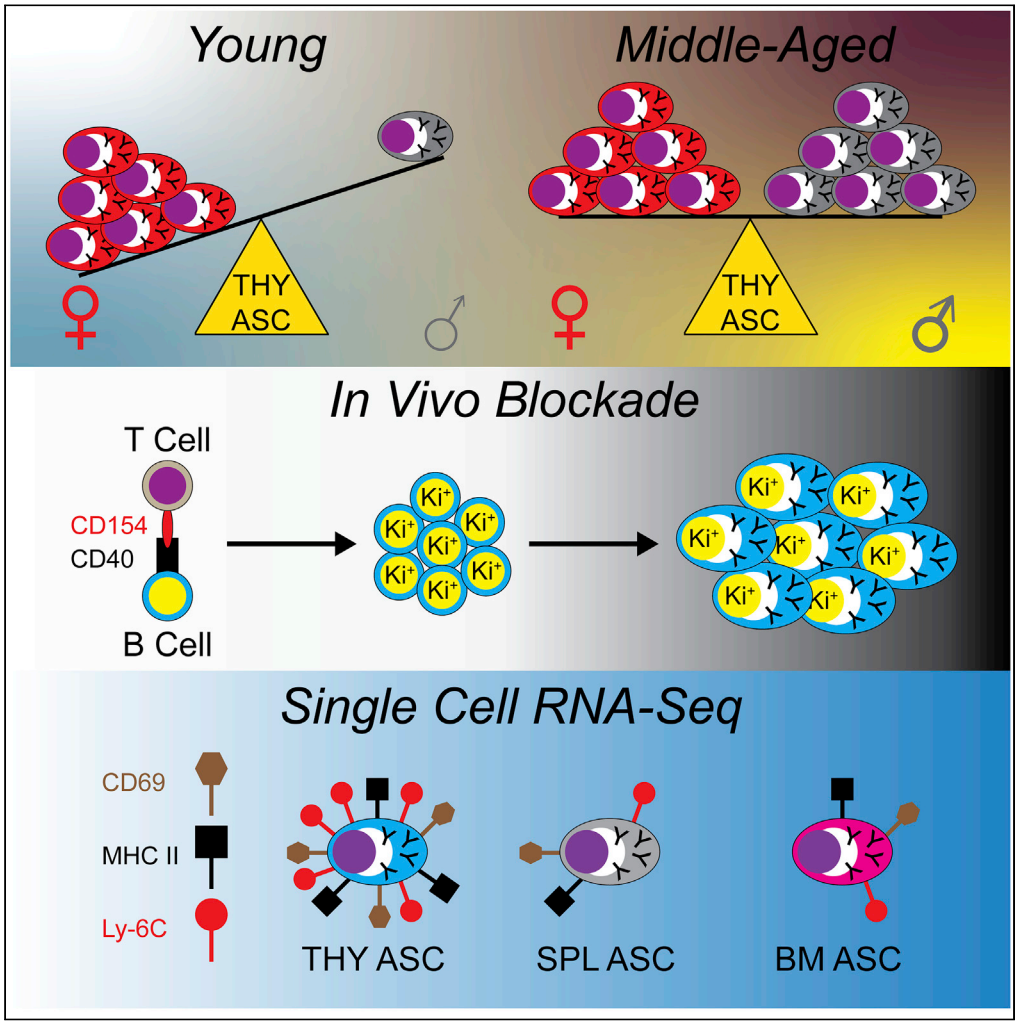

KimAnh T. Pioli, Kin H. Lau, Peter D. Pioli

peter.pioli@usask.ca

Highlights

Thymus ASCs are selectively increased in young female Prdm1-eYFP mice

Thymus ASCs contain a CD154(CD40L) dependent Ki-67^{+} plasmablast population

Ectopic *in vivo* CD40 ligation does not increase total thymus ASC numbers

Thymus ASCs possess an interferon responsive gene signature

Pioli et al., iScience *26*, 106223
March 17, 2023
https://doi.org/10.1016/j.isci.2023.106223

iScience

CellPress
OPEN ACCESS

Article

Thymus antibody-secreting cells possess an interferon gene signature and are preferentially expanded in young female mice

KimAnh T. Pioli,[1] Kin H. Lau,[2] and Peter D. Pioli[1,3,*]

SUMMARY

Antibody-secreting cells (ASCs) are key contributors to humoral immunity through immunoglobulin production and the potential to be long-lived. ASC persistence has been recognized in the autoimmune thymus (THY); however, only recently has this population been appreciated in healthy THY tissue. We showed that the young female THY was skewed toward higher production of ASCs relative to males. However, these differences disappeared with age. In both sexes, THY ASCs included Ki-67^{+} plasmablasts which required CD154(CD40L) signals for their propagation. Single cell RNA-sequencing revealed that THY ASCs were enriched for an interferon responsive transcriptional signature relative to those from bone marrow and spleen. Flow cytometry confirmed that THY ASCs had increased levels of Toll-like receptor 7 as well as CD69 and major histocompatibility complex class II. Overall, we identified fundamental aspects of THY ASC biology which may be leveraged for future in depth studies of this population in both health and disease.

INTRODUCTION

Humoral, or antibody (Ab) mediated, immunity is essential in preventing infection from a wide variety of bacterium and viruses. This is in part because of the many functions of Ab molecules which include neutralization, opsonization, and activation of various effector cell types.[1] Based on namesake alone, it is no surprise that antibody-secreting cells (ASCs) are key contributors to the humoral immune system. Not only do these cells continuously secrete Abs[2] but a segment of the population has been shown to be long-lived in both mice[2–5] and humans.[6–8]

ASCs also possess numerous immunomodulatory roles which can be partially attributed to their ability to secrete cytokines.[9–11] For instance, ASC production of interleukin-10 (IL-10) has been associated with the suppression of neuroinflammation[12] and attenuation of the response to *Salmonella* infection.[13] In the latter case, this has been linked with expression of LAG-3.[13] In contrast, ASCs have also demonstrated production of proinflammatory cytokines such as tumor necrosis factor-alpha (TNF-α)[14] and IL-17[15] which play roles in gut homeostasis and response to *Trypanosoma cruzi* infection, respectively. Aside from the above, ASCs influence homeostatic processes such as hematopoiesis.[16,17] Although hematopoietic regulatory capacity has been ascribed to bone marrow (BM) ASCs, whether ASCs regulate hematopoietic processes in other organs such as the thymus (THY) remains to be determined.

Historically, the presence of ASCs in the human THY has been associated with autoimmune diseases such as myasthenia gravis.[18–20] In addition, mouse models of lupus have demonstrated disease-associated expansion of THY ASCs.[21] In these instances, THY ASCs are continuously produced and secrete pathogenic autoantibodies. Aside from providing clues as to autoimmune etiology, studying ASCs in the healthy THY may reveal important insights as to their everyday function. In this regard, human studies have identified ASC populations in the neonatal THY which are preserved and potentially expanded over the course of aging.[22,23] Histological analyses in humans have shown these cells to be located within the perivascular space (PVS) of the THY medulla[22,23] and recent RNA-sequencing (RNA-seq) experiments have inferred an intra-THY development of these cells.[22] From a functional standpoint, THY ASC Abs have been shown to be virally and bacterially reactive,[22,23] but it is unclear as to what percentages these reactivities occupy within the total THY ASC Ab repertoire. This is of particular interest because the human THY is thought to be enriched

[1]Department of Biochemistry, Microbiology and Immunology, College of Medicine, University of Saskatchewan, Saskatoon, SK S7N5E5, Canada

[2]Bioinformatics and Biostatistics Core, Van Andel Institute, Grand Rapids, MI 49503, USA

[3]Lead contact

*Correspondence: peter.pioli@usask.ca

https://doi.org/10.1016/j.isci.2023.106223

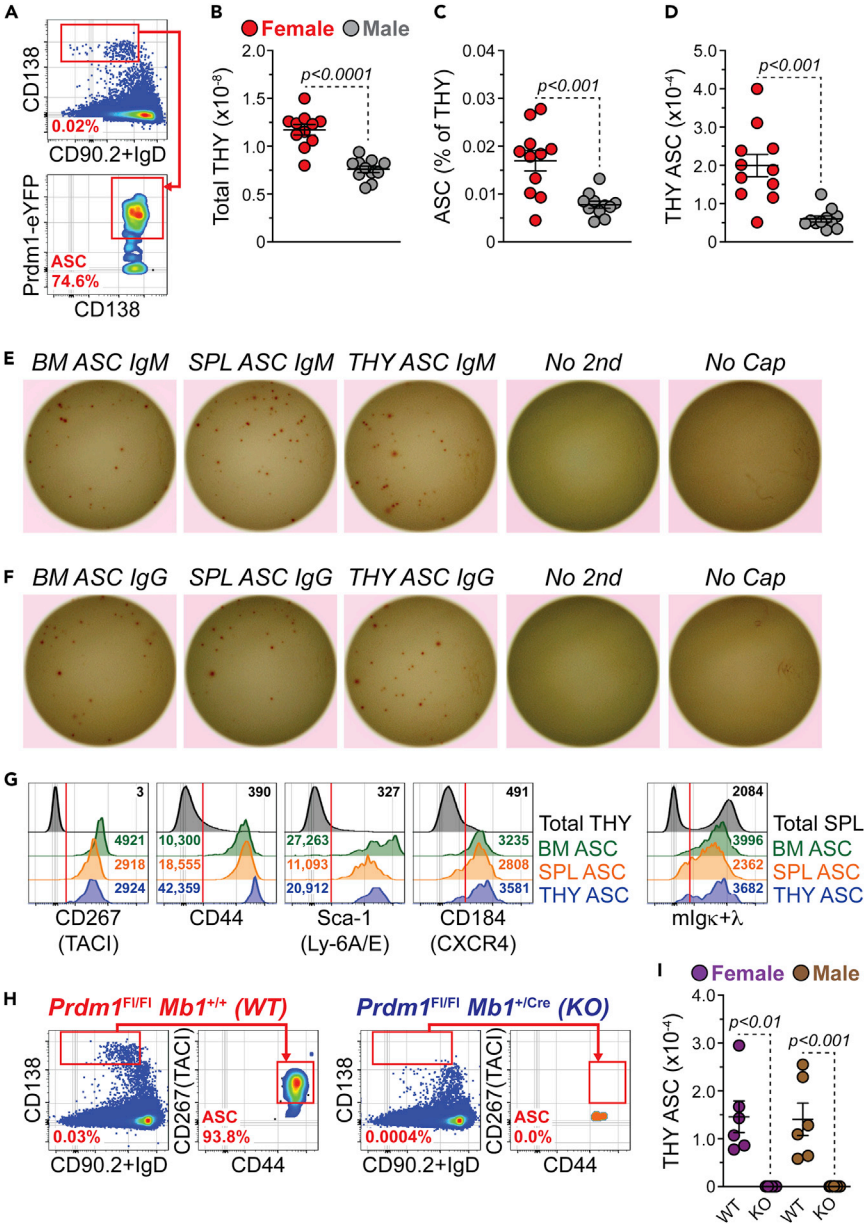

Figure 1. Thymus antibody-secreting cells are preferentially increased in young female thymus, related to Figure S1

(A) Flow cytometry plots depicting representative gating of total ASCs from the THY. Cells pre-gated on total singlets. Numbers in plots represent percentages within the immediate parent population.

(B) Total THY cell numbers.

(C) Percentages of THY ASCs.

(D) Numbers of THY ASCs.

(E and F) Representative ELISpot images of (E) IgM and (F) total IgG of 100 sorted BM, SPL and THY ASCs per well. Data shown for males. Wells assayed without secondary reagents (No second) or capture Ab (No Cap) were seeded with SPL ASCs. Experiments were reproduced with female ASCs.

(G) Flow cytometry overlays showing CD267(TACI), CD44, Sca-1(Ly-6A/E), CD184(CXCR4) and mIgκ+λ staining on the surface of ASCs from BM, SPL and THY. Total THY or SPL is shown for comparison. Red vertical lines added to histograms show cut-offs for positive staining. Numbers in plots indicate gMFI.

(H) Flow cytometry plots showing representative gating of THY ASCs from *Prdm1*$^{Fl/Fl}$*Mb1*$^{+/+}$ WT and *Prdm1*$^{Fl/Fl}$*Mb1*$^{+/Cre}$ KO mice. Numbers in plots represent percentages within the immediate parent population.

Figure 1. *Continued*
(I) Numbers of THY ASCs from 3 to 5-mo.-old Prdm1 WT and KO mice.
(B–D and I) Symbols represent individual mice. Horizontal lines represent mean ± SEM. Unpaired Student's t-test for inter-sex comparisons. Paired Student's t-test for intra-sex comparisons.
(B–D) Female: n = 11; Male: n = 11. (I) Female WT: n = 6; Female KO: n = 6; Male WT: n = 6; Male KO: n = 8.

for autoreactive B cell clones[24] and experiments using mice have shown the ability of autoreactive THY B cells to class switch following their interactions with developing T lymphocytes.[25] Along these lines, recent work using BALB/c mice demonstrated the presence of IgE-secreting THY ASCs which were critical to mast cell development.[26] As informative as these studies are, they failed to consider potential sex differences and provided only a limited comparison of THY ASCs to their peripheral counterparts. The former point is relevant because numerous sex differences exist within the immune system.[27]

In this report, we compared the development and phenotypic characteristics of female and male THY ASCs versus their cellular equivalents in the BM and spleen (SPL). Production of THY ASCs favored females in youth (3-month (mo.)-old mice) and reached similarity between the sexes by middle age (12-mo.-old), an observation which was unique when compared to BM and SPL. As in the SPL, the THY possessed a Ki-67^{+} plasmablast (PB) population which was significantly reduced on the *in vivo* blockade of CD154(CD40L) signaling. Like their peripheral counterparts, THY ASCs also required the expression of BLIMP-1 as its deletion ablated this population. Via single cell RNA-seq (scRNA-seq), we identified three developmental lineages which were shared between ASCs isolated from the BM, SPL and THY. However, closer inspection of VDJ and transcriptional patterns revealed an immunoglobulin repertoire and interferon (IFN) responsive gene signature that was unique to THY ASCs and included increased expression of genes such as *Tlr7* and *Ly6c2*. Overall, these data provide a valuable resource to be leveraged for future exploration of THY ASCs.

RESULTS

Young female mice have increased numbers of THY ASCs relative to males

Previous work has identified the presence of ASCs in the THY of humans[22,23] and mice[21,28]; however, they remain to be fully characterized. To begin addressing this deficiency, we used 3-mo.-old Prdm1-enhanced yellow fluorescence protein (eYFP) reporter mice to examine ASCs in the THY. These mice possess a bacterial artificial chromosome (BAC) that expresses enhanced yellow fluorescent protein (eYFP) downstream of the *Prdm1* gene[29] and can be used to identify ASCs when combined with the surface expression of selected proteins. Via flow cytometry, ASCs were identified as CD138^{HI} IgD$^{-/LO}$ CD90.2$^{-/LO}$ Prdm1-eYFP^{+} (Figure 1A). In agreement with previous studies,[30,31] 3-mo.-old female mice had increased overall cellularity in the THY compared to age-matched males (Figure 1B). Percentages (Figure 1C) and numbers (Figure 1D) of ASCs were both significantly increased in female THY relative to male mice. The BM and SPL did not demonstrate similar phenotypes (Figures S1A–S1F) lending specificity to observations in the THY.

To functionally validate THY ASCs, we purified them via fluorescence-activated cell sorting (FACS) (Figures S1G and S1H) and performed enzyme-linked immunosorbent spot (ELISpot) assays for IgM (Figure 1E) and total IgG (Figure 1F). As with BM and SPL, the THY ASC population possessed cells capable of IgM or IgG secretion, thus confirming their functional identity (Figures 1E, 1F, and S1I). Further comparison to BM and SPL ASCs showed that THY ASCs expressed ASC-associated proteins such as CD267(TACI),[32,33] CD44,[34–36] Sca-1(Ly-6A/E)[37] and CD184(CXCR4)[33] (Figure 1G). In addition, THY ASCs expressed membrane immunoglobulin (mIgκ+λ) like that observed for ASCs from the BM and SPL (Figure 1G).[17,38,39] In some instances, organ-to-organ expression differences were evident (Figures S1J–S1N). For example, BM ASCs expressed the highest amounts of CD267(TACI) as assessed by flow cytometric geometric mean fluorescence intensity (gMFI) (Figure S1J), whereas THY ASCs expressed the highest levels of CD44 (Figure S1K).

Finally, BLIMP-1, encoded for by *Prdm1*, is a key regulator of ASC differentiation and function.[40–42] For instance, the genetic ablation of *Prdm1* in B cells leads to the loss of ASCs in the SPL following immunization.[43] To determine the importance of BLIMP-1 for the formation of THY ASCs, we bred mice with a conditional allele of *Prdm1*[43] to a strain possessing the B cell specific Mb1(Cd79a)-Cre.[44] Here we performed analyses using 3–5-mo.-old mice which were not age matched. In the absence of the Prdm1-eYFP reporter, THY ASCs were identified as CD138^{HI} IgD$^{-/LO}$ CD90.2$^{-/LO}$ CD267(TACI)$^{+}$ CD44^{+} (Figure 1H). Mice with the

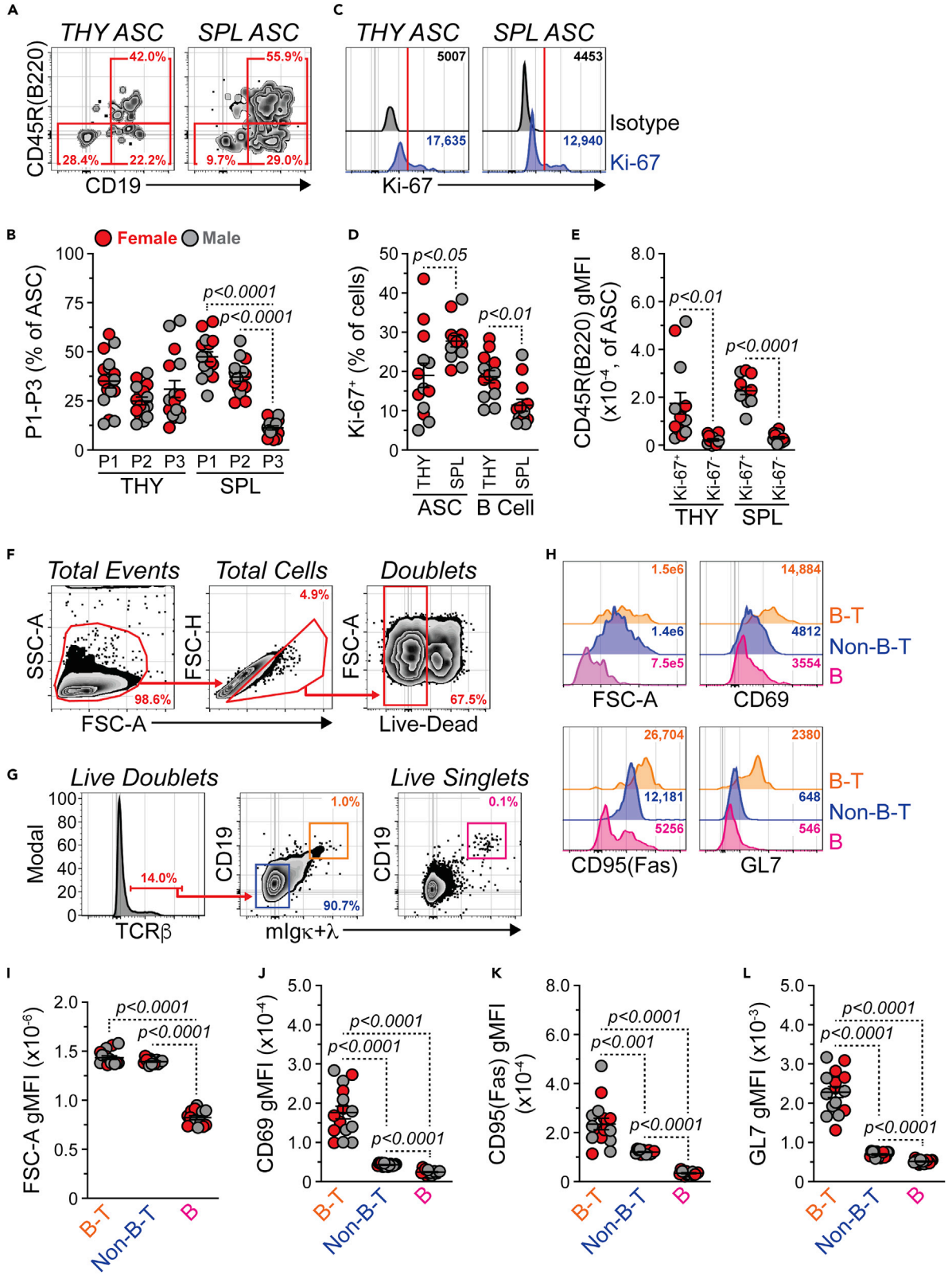
A
THY ASC
SPL ASC
CD45R(B220)
42.0%
55.9%
28.4%
22.2%
9.7%
29.0%
CD19
C
THY ASC
SPL ASC
5007
4453
17,635
12,940
Isotype
Ki-67
Ki-67
B
Female
Male
P1-P3 (% of ASC)
p<0.0001
p<0.0001
P1 P2 P3 P1 P2 P3
THY
SPL
D
Ki-67+ (% of cells)
p<0.05
p<0.01
THY SPL THY SPL
ASC
B Cell
E
CD45R(B220) gMFI (x10-4, of ASC)
p<0.01
p<0.0001
Ki-67+ Ki-67- Ki-67+ Ki-67-
THY
SPL
F
Total Events
Total Cells
Doublets
SSC-A
FSC-A
FSC-H
4.9%
98.6%
FSC-A
FSC-A
Live-Dead
67.5%
G
Live Doublets
Live Singlets
Modal
14.0%
TCRβ
CD19
1.0%
90.7%
mIgκ+λ
CD19
0.1%
H
1.5e6
1.4e6
7.5e5
FSC-A
14,884
4812
3554
CD69
B-T
Non-B-T
B
26,704
12,181
5256
CD95(Fas)
2380
648
546
GL7
B-T
Non-B-T
B
I
FSC-A gMFI (x10-6)
p<0.0001
p<0.0001
B-T
Non-B-T
B
J
CD69 gMFI (x10-4)
p<0.0001
p<0.0001
p<0.0001
B-T
Non-B-T
B
K
CD95(Fas) gMFI (x10-4)
p<0.0001
p<0.001
p<0.0001
B-T
Non-B-T
B
L
GL7 gMFI (x10-3)
p<0.0001
p<0.0001
p<0.0001
B-T
Non-B-T
B

Figure 2. Thymic antibody-secreting cells contain plasmablasts, related to Figure S2

(A) Flow cytometry plots depicting representative P1-P3 gating of THY and SPL ASCs. Numbers in plots represent percentages within the immediate parent population.

(B) Percentages of P1-P3 within THY and SPL ASCs.

(C) Flow cytometry overlays showing isotype control and Ki-67 intracellular staining of THY and SPL ASCs. Red vertical lines added to histograms show cut-offs for positive staining. Numbers in plots indicate gMFI.

(D) Percentages of Ki-67$^+$ cells within ASCs and B cells from THY and SPL.

(E) CD45R(B220) gMFI for Ki-67$^+$ and Ki-67$^-$ THY and SPL ASCs.

(F) Flow cytometry plots showing gating of THY live doublets. Numbers in plots represent percentages within the immediate parent population.

(G) Flow cytometry plots depicting identification of CD19$^+$ mIgκ+λ$^+$ cells within TCRβ$^+$ live doublets and total live singlets within the THY. Numbers in plots represent percentages within the immediate parent population.

(H) Flow cytometry overlays showing FSC-A (forward scatter, cell size), CD69, CD95(Fas) and GL7 analysis of B cell-T cell (B-T) doublets, non-B-T cell (Non-B-T) doublets and B cell (B) singlets. Numbers in plots indicate gMFI.

(I–L) gMFIs for (I) FSC-A, (J) CD69, (K) CD95(Fas) and (L) GL7 for THY B-T doublets, Non-B-T doublets and B singlets. (B, D, E, I–L) Symbols represent individual mice. Horizontal lines represent mean ± SEM.

(B) One-way ANOVA with Tukey's correction. Female: n = 8; Male: n = 8.

(D and E) Paired Student's t-test. Female: n = 7; Male: n = 6.

(I–L) One-way ANOVA with Tukey's correction. Female: n = 7; Male: n = 8.

Prdm1$^{Fl/Fl}$*Mb1*$^{+/+}$ genotype were wildtype (WT) and possessed a distinct ASC population (Figure 1H). This population was lost in *Prdm1*$^{Fl/Fl}$*Mb1*$^{+/Cre}$ ASC knockout (KO) mice (Figures 1H and 1I) demonstrating the conserved reliance on BLIMP-1 for the generation of THY ASCs. Taken together, these data support the existence of *bona fide* ASCs which are preferentially increased in the young female THY of Prdm1-eYFP mice.

THY ASCs contain a plasmablast population and are not recently immigrated

Using cell surface markers such as CD45R(B220) and CD19, ASCs in the BM and SPL can be subdivided into 3 populations. Population 1 is CD45R(B220)$^+$ CD19$^+$ and includes Ki-67$^+$ PBs, whereas populations 2 and 3 are B220$^-$ CD19$^+$ and B220$^-$ CD19$^-$, respectively.[3,45] These latter two populations represent more mature plasma cells. To investigate these populations in the THY, we performed flow cytometry on ASCs from 3- to 5-mo.-old female and male C57BL/6J mice with ASCs identified as in Figure 1H. THY ASCs were relatively balanced between compartments P1-P3 (Figures 2A and 2B). In contrast, SPL ASCs were composed largely of populations P1 and P2 (Figures 2A and 2B). To further confirm the existence of THY ASCs with a PB phenotype, we performed intracellular staining for the proliferation marker Ki-67 (Figure 2C). A wide range of Ki-67 positivity existed within the THY ASC population (Figure 2D). As a whole, the percentage of Ki-67$^+$ ASCs was significantly lower in the THY compared to the SPL (Figure 2D) which agreed with the differential skewing of P1-P3 amongst the organs. In contrast, THY B cells (CD45R(B220)$^+$ CD19$^+$ CD138$^{-/LO}$) had a slightly increased percentage of Ki-67$^+$ cells relative to those in the SPL (Figure 2D). Analysis of Ki-67$^+$ ASCs in THY and SPL demonstrated significantly higher CD45R(B220) expression compared to Ki-67$^-$ ASCs. This confirmed that CD45R(B220) could be used as a marker to enrich for PBs within the THY ASC compartment.

PBs are generally considered to be short-lived[3] and their presence in the THY could be indicative of a local B cell response. This would agree with previous work which has shown THY B cells to possess an activated phenotype.[46,47] To lend support to this notion, we evaluated the THY for B cell-T cell conjugates by flow cytometrically analyzing live cell doublets (Figure 2F) similar to previous studies.[48] Using this method, we were able to identify putative B cell-T cell (B-T) conjugates that were TCRβ$^+$ CD19$^+$ mIgκ+λ$^+$ (Figure 2G). As expected, both B-T doublets and TCRβ$^+$ CD19$^-$ mIgκ+λ$^-$ (Non-B-T) doublets had increased cell size (FSC-A) relative to CD19$^+$ mIgκ+λ$^+$ (B) singlets (Figures 2G–2I). When compared to Non-B-T doublets and B singlets, B-T doublets possessed increased levels of CD69, CD95(Fas) and GL7 which suggested an activated phenotype (Figures 2H and 2J–2L).

In line with the above, recent studies in BALB/c mice have utilized techniques such as parabiosis and intravenous (i.v.) Ab labeling to support that THY ASCs are not recent immigrants and are generated locally.[26] To test this in mice on the C57BL/6 background, we injected PBS (PBS) or 1 μg of αCD45-PE Abs i.v. into 3-mo.-old Prdm1-eYFP mice (Figure S2A). After 5 min (min.) or 24 h, we euthanized mice and analyzed the distribution of αCD45-PE staining within the peripheral blood (BLD), BM, SPL and THY. αCD45-PE labeled cells within a tissue are indicative of localization within the tissue vasculature or having trafficked the bloodstream during the labeling period.[49–51] As expected, cells from the BLD of mice infused with

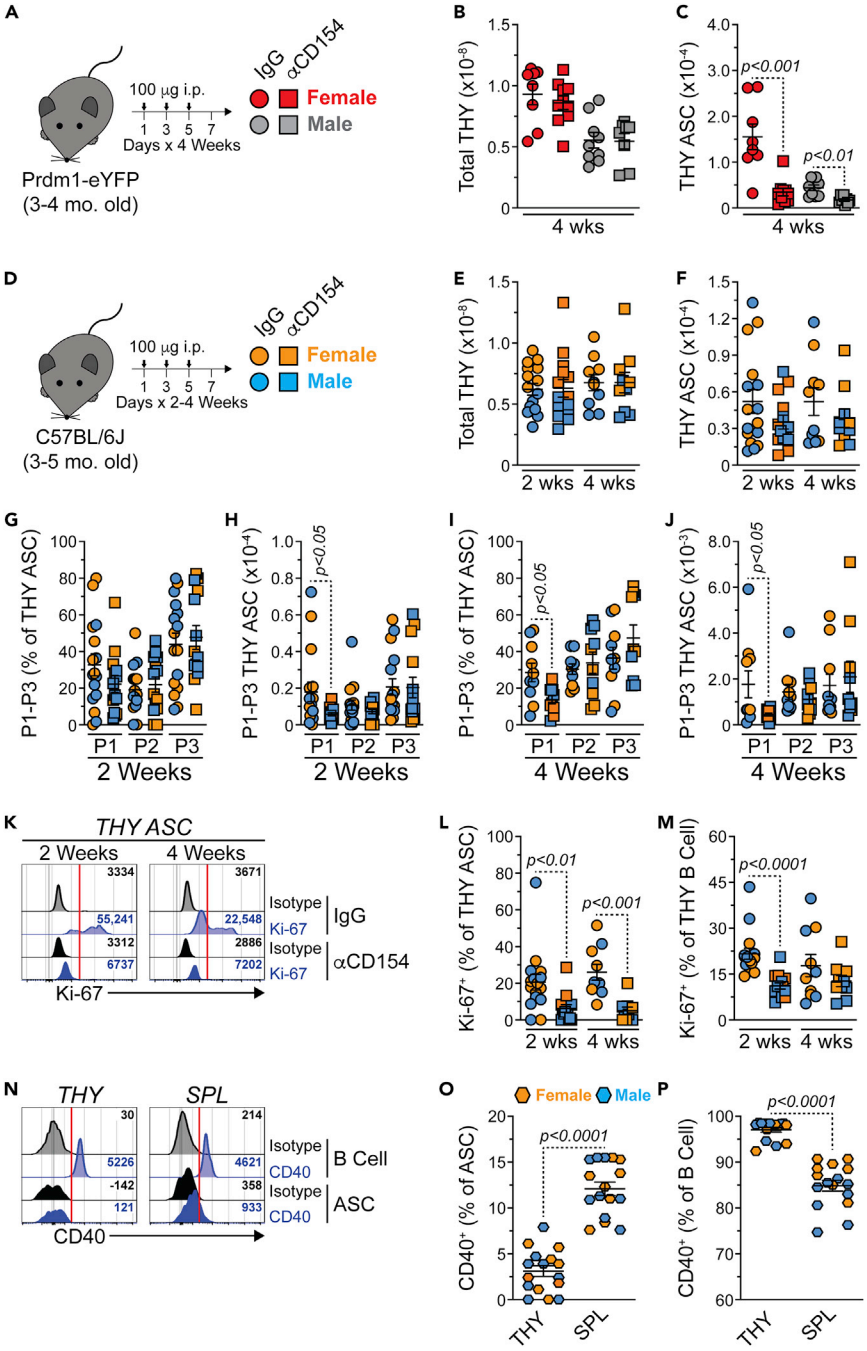

Figure 3. Blockade of CD154(CD40L)-derived signals reduces proliferative antibody-secreting cells in the thymus, related to Figure S3

(A) Young (3-4-mo.-old) Prdm1-eYFP female and male mice received 1200 µg total of hamster IgG isotype control or anti-mouse CD154(CD40L) (MR-1) Abs. Administration was split evenly amongst 12-total i.p. injections (100 µg per injection, 100 µL volume) over a 4-week span.

(B and C) Total THY and THY ASC numbers in Prdm1-eYFP mice treated with hamster IgG isotype control or anti-mouse CD154 Abs for 4 weeks.

(D) Young (3-5-mo.-old) C57BL/6J female and male mice were treated as in (A) over a 2- or 4-week span.

(E and F) Total THY and THY ASC numbers in C57BL/6J mice treated with hamster IgG isotype control or anti-mouse CD154 Abs for 2 or 4 weeks.

Figure 3. *Continued*

(G and H) C57BL/6J P1-P3 (G) percentages within THY ASCs and (H) cell numbers following 2 weeks of IgG isotype control or anti-mouse CD154 treatment.

(I and J) C57BL/6J P1-P3 (I) percentages within THY ASCs and (J) cell numbers following 4 weeks of IgG isotype control or anti-mouse CD154 treatment.

(K) Flow cytometry overlays showing isotype control and Ki-67 intracellular staining of THY ASCs from mice following 2 or 4 weeks of IgG isotype control or anti-mouse CD154 treatment. Red vertical lines added to histograms show cut-offs for positive staining. Numbers in plots indicate gMFI.

(L and M) Percentages of Ki-67$^+$ cells within THY (L) ASCs and (M) B cells following 2 or 4 weeks of IgG isotype control or anti-mouse CD154 treatment.

(N) Flow cytometry overlays showing isotype control and CD40 surface staining of ASCs and B cells from THY and SPL of unmanipulated C57BL/6J mice. Red vertical lines added to histograms show cut-offs for positive staining. Numbers in plots indicate gMFI.

(O and P) Percentages of CD40$^+$ cells within THY and SPL (O) ASCs and (P) B cells.

(B, C, E–J, L, M, O, and P) Symbols represent individual mice. Horizontal lines represent mean ± SEM.

(B and C) Unpaired Student's t-test. Female IgG: n = 8; Female αCD154: n = 10; Male IgG: n = 9; Male αCD154: n = 8.

(E–J, L, and M) Unpaired Student's t-test. 2 weeks Female IgG: n = 8; 2 weeks Female αCD154: n = 7; 2 weeks Male IgG: n = 8; 2 weeks Male αCD154: n = 7; 4 weeks Female IgG: n = 5; 4 weeks Female αCD154: n = 5; 4 weeks Male IgG: n = 5; 4 weeks Male αCD154: n = 5.

(O and P) Paired Student's t-test. Female: n = 8; Male: n = 8.

αCD45-PE for 5 min possessed >99% labeling demonstrating the efficacy of our protocol (Figure S2B). αCD45-PE labeling of ASCs revealed organ specific staining patterns (Figure S2C). In agreement with previous studies,[3,26] BM ASCs demonstrated low levels of labeling (~11.8%) after 5 min, whereas that of SPL ASCs was more extensive (~42.7%) (Figure S2D). In the THY, 0% of ASCs were labeled after 5 min (Figure S2D). At 24 h, we observed high percentages of αCD45-PE$^+$ ASCs in the BM (~41.0%) and SPL (~58.8%); however, THY ASCs remained unlabeled (Figure S2D). The lack of αCD45-PE staining on THY ASCs was not due to absence of CD45 as *ex vivo* staining with αCD45-APC demonstrated similarities in CD45 expression amongst ASCs from all 3 organs (Figure S2E). In total, these results demonstrate the presence of PBs within the THY ASC population and suggest that THY ASCs are not recently immigrated.

CD154(CD40L)-derived signals are required for production of THY PBs

The context in which a B cell is activated can influence ASC differentiation. For example, ASCs can be generated via either a T cell independent or T cell dependent immune response.[52] It has been shown that THY B cells class switch when activated in the presence of T cell-derived signals and genetic ablation of TCRα, MHC II or CD40 led to a significant loss of class switched THY B cells.[25] As such, we hypothesized that inhibition of B cell-T cell signaling would lead to a reduction in THY ASCs. To test this, cohorts of 3–4-mo.-old female and male Prdm1-eYFP mice were treated intraperitoneally (i.p.) with isotype control IgG or αCD154(CD40L) blocking Abs for 1 month (Figures 3A and S3A). Subsequently, mice were euthanized and ASC populations were assessed. CD154 blockade did not affect total THY cell numbers (Figure 3B) but it did lead to a significant reduction in THY ASCs (Figure 3C). For comparison, 1-month inhibition of CD154 reduced total SPL numbers (Figure S3B) while also having decreased the total ASC population (Figure S3C). The above effects were evident for both sexes.

We hypothesized that any loss of ASCs would largely be because of a decrease in the proliferative, and presumably short-lived, PB compartment. As such, we repeated the above experiments and assessed ASC populations at both 2- and 4-weeks following isotype control or αCD154 administration (Figures 3D–3M and S3D–S3M). Because of availability, these experiments were performed with 3-5-mo.-old C57BL/6J mice purchased and used directly from The Jackson Laboratory. As such, these mice were not strictly age or litter matched as in previous experiments. Within the THY, total cellularity was unaffected by the loss of CD154 signals (Figure 3E) and there was a trend toward the reduction of total THY ASCs in mice treated with αCD154 Abs for 2- and 4-weeks (Figure 3F). Examination of THY ASC populations P1-P3 demonstrated little difference in percentages after 2 weeks of blockade (Figure 3G). However, THY P1 was significantly reduced in numbers at 2 weeks (Figure 3H). At 4 weeks post αCD154 treatment, THY P1 was significantly decreased in both percentages and absolute numbers. (Figures 3I and 3J). Perhaps not surprisingly, we observed a significant decrease of proliferating Ki-67$^+$ THY ASCs in mice injected with αCD154 Abs (Figures 3K and 3L). Impairment of CD154 also reduced the percentage of Ki-67$^+$ THY B cells which was most evident at 2 weeks (Figure 3M). Results in the SPL were largely similar albeit with greater penetrance (Figures S3E–S3M). Evaluation of CD40 expression (Figure 3N) demonstrated minimal protein

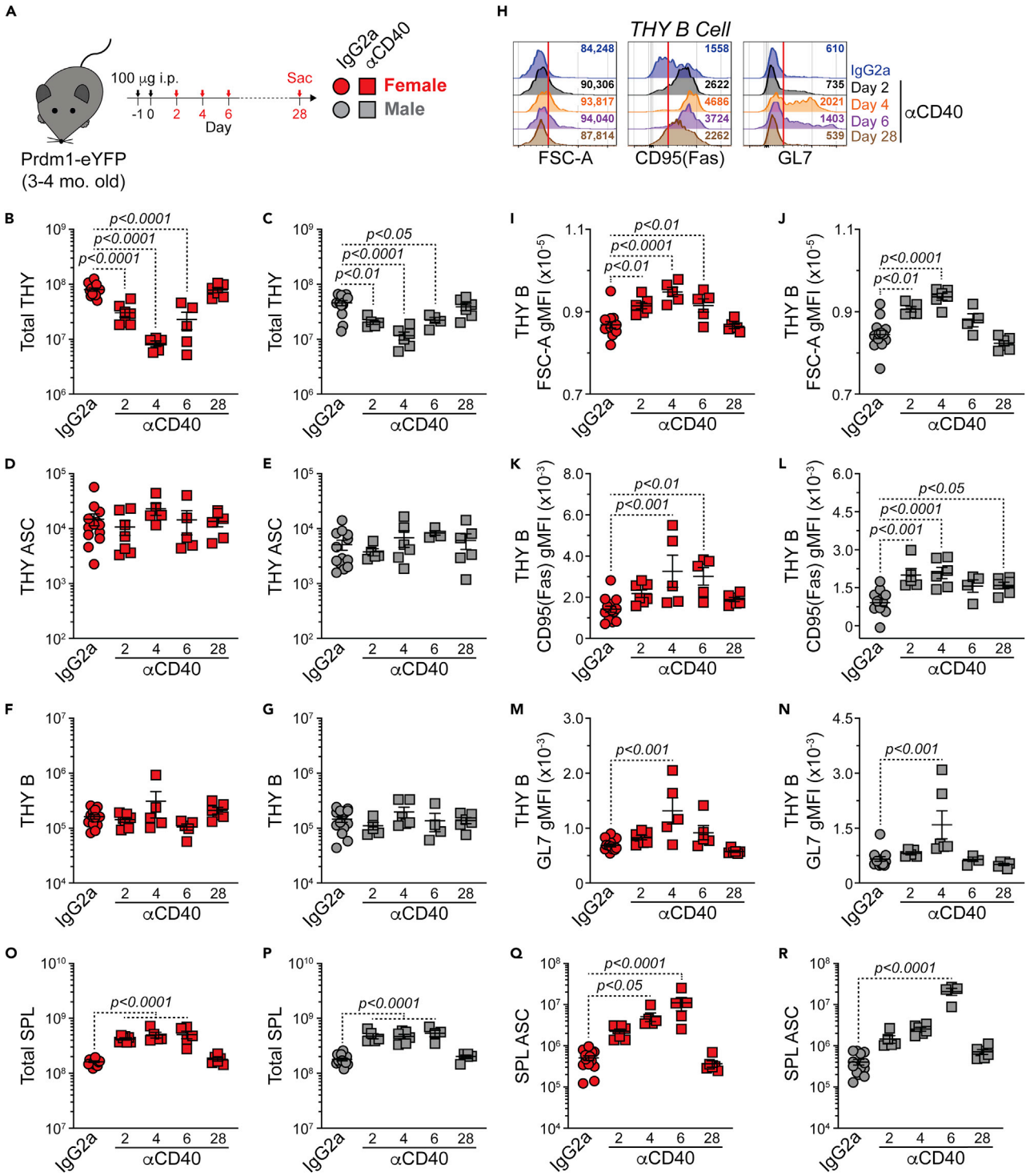

Figure 4. Ectopic CD40 stimulation does not increase thymus antibody-secreting cell numbers

(A) Young (3-4-mo.-old) Prdm1-eYFP female and male mice received a total of 200 µg of rat IgG2a isotype control or anti-mouse CD40 (FGK4.5/FGK45) antibodies. Doses (100 µg per injection, 100 µL volume) were administered i.p. on days −1 and 0. Animals were euthanized 2, 4, 6 and 28 days after injection.

(B–G) Numbers of (B and C) total THY, (D and E) THY ASCs and (F and G) THY B cells from female and male IgG2a- or αCD40-treated mice.

(H) Flow cytometry overlays showing FSC-A, CD95(Fas) and GL7 analysis of THY B cells. Red vertical lines added to histograms as a reference for shift in gMFI. Numbers in plots indicate gMFI.

(I–N) gMFIs for (I and J) FSC-A, (K and L) CD95(Fas) and (M and N) GL7 for THY B cells from female and male IgG2a- or αCD40-treated mice.

Figure 4. *Continued*

(O–R) Numbers of (O and P) total SPL and (Q and R) SPL ASCs from female and male IgG2a- or αCD40-treated mice. (B–G and I–R) Symbols represent individual mice. Horizontal lines represent mean ± SEM. IgG2a data represent pooled control mice from days 2, 4, 6 and 28. One-way ANOVA with Dunnett's correction. All comparisons made against IgG2a controls. Female IgG2a: n = 13; Female αCD40 day 2: n = 7; Female αCD40 day 4: n = 5; Female αCD40 day 6: n = 5; Female αCD40 day 28: n = 6; Male IgG2a: n = 13; Male αCD40 day 2: n = 5; Male αCD40 day 4: n = 6; Male αCD40 day 6: n = 4; Male αCD40 day 28: n = 6.

on the surface of THY ASCs which was reduced when compared to ASCs from the SPL (Figure 3O). In contrast, THY B cells possessed increased levels of CD40 compared to their splenic counterparts (Figure 3P). Based on CD40 expression, most of the effects observed in the THY were likely driven via the loss of CD40 signaling by THY B cells. Overall, these data indicate the importance of CD154 signals in the production and/or maintenance of THY ASCs with a particular emphasis on the Ki-67^{+} PB population.

In vivo CD40 activation does not increase numbers of total THY ASCs

Given the previous data, we wanted to know if ectopic CD154(CD40L):CD40 signals would be sufficient to drive expansion of THY ASCs. To address this, 3-4-mo.-old female and male Prdm1-eYFP mice were treated i.p. with isotype control IgG2a or αCD40 agonistic Abs on days −1 and 0 and then euthanized on days 2, 4, 6 and 28 post-injection (Figure 4A). Data from isotype control treated mice were pooled owing to no clear variation between timepoints. Evaluation of female and male THY showed a transient decrease in overall cellularity which recovered by day 28 after αCD40 injection (Figures 4B and 4C). The THY ASC population showed no change in cell numbers across the time course (Figures 4D and 4E). This could have been because of the lack of B cell activation in the THY. To eliminate this possibility, the THY B cell compartment was also analyzed. CD40 stimulation did not alter the overall number of THY B cells (Figures 4F and 4G); however, we did observe changes that were indicative of activation. These included increased cell size (FSC-A), CD95(Fas) and GL7 (Figures 4H–4N). For the most part, these changes were temporally regulated with a peak at days 4–6 and subsequent return to baseline by day 28. To confirm that our protocol was sufficient to generate ASCs, at least in other organs, we examined the effects of αCD40 treatment in the SPL. In both sexes, SPL cell numbers were increased (days 2–6) following stimulation (Figures 4O and 4P). This was in part because of SPL B cell expansion (data not shown). Importantly, ASCs were also increased in the short term on CD40 ligation (Figures 4Qand 4R). Overall, these data suggest that αCD40 ligation *in vivo* can transiently increase ASCs. However, this is tissue restricted as ectopic CD40 stimulation alone does not expand THY ASCs.

ASC subsets exist with divergent gene ontology associations

The above data indicated that THY ASCs were potentially divergent when compared to those from the BM and SPL. To better understand these differences, we FACS-purified ASCs from the BM, SPL and THY and performed scRNA-seq to assess single cell gene expression (scGEX) as well as VDJ (scVDJ) usage via the 10x Genomics platform (Figure 5A). This was done with cells separately isolated from pools of 3 female and 3 male 3-mo.-old Prdm1-eYFP mice. Similar to previous data,[22,53] expression of *Sdc1*, *Prdm1*, *Xbp1* and *Ell2* was readily detectable amongst ASCs (Figures 5B and S4A) validating cell identity. Clustering of ASCs led to the classification of 12 clusters labeled 0–11 (Figure 5C). Although there was some variability between the sexes regarding cluster contribution to total ASCs, Cluster 0 was a consistent majority within the THY of both female and male mice (Figure 5D). In contrast, BM and SPL showed a greater prevalence for "minor" clusters such as Cluster 4 (Figure 5D).

To better understand transcriptional differences between clusters, we utilized the *scran* package to identify marker genes that were significantly enriched in a cluster as indicated by an area under the curve (AUC) > 0.60 and false discovery rate (FDR) < 0.05 (Table S1). The AUC represents the probability that expression of a given gene from a cell in a particular cluster is greater than any random cell from another cluster. When comparing clusters, Cluster 11 possessed the most marker genes (4,782 total, Figure S4B and Table S1). We observed a dichotomy in terms of the contribution of Ig versus non-Ig genes to the total number of marker genes. Clusters 0-1 and 7-8 were skewed toward Ig marker genes (>30% of total genes, Figure S4B and Table S1) whereas Clusters 3, 5 and 9-11 were dominated by non-Ig genes (>95% of total genes, Figure S4B and Table S1). This difference was mostly because of a lack of non-Ig marker genes in clusters 0-1 and 7-8.

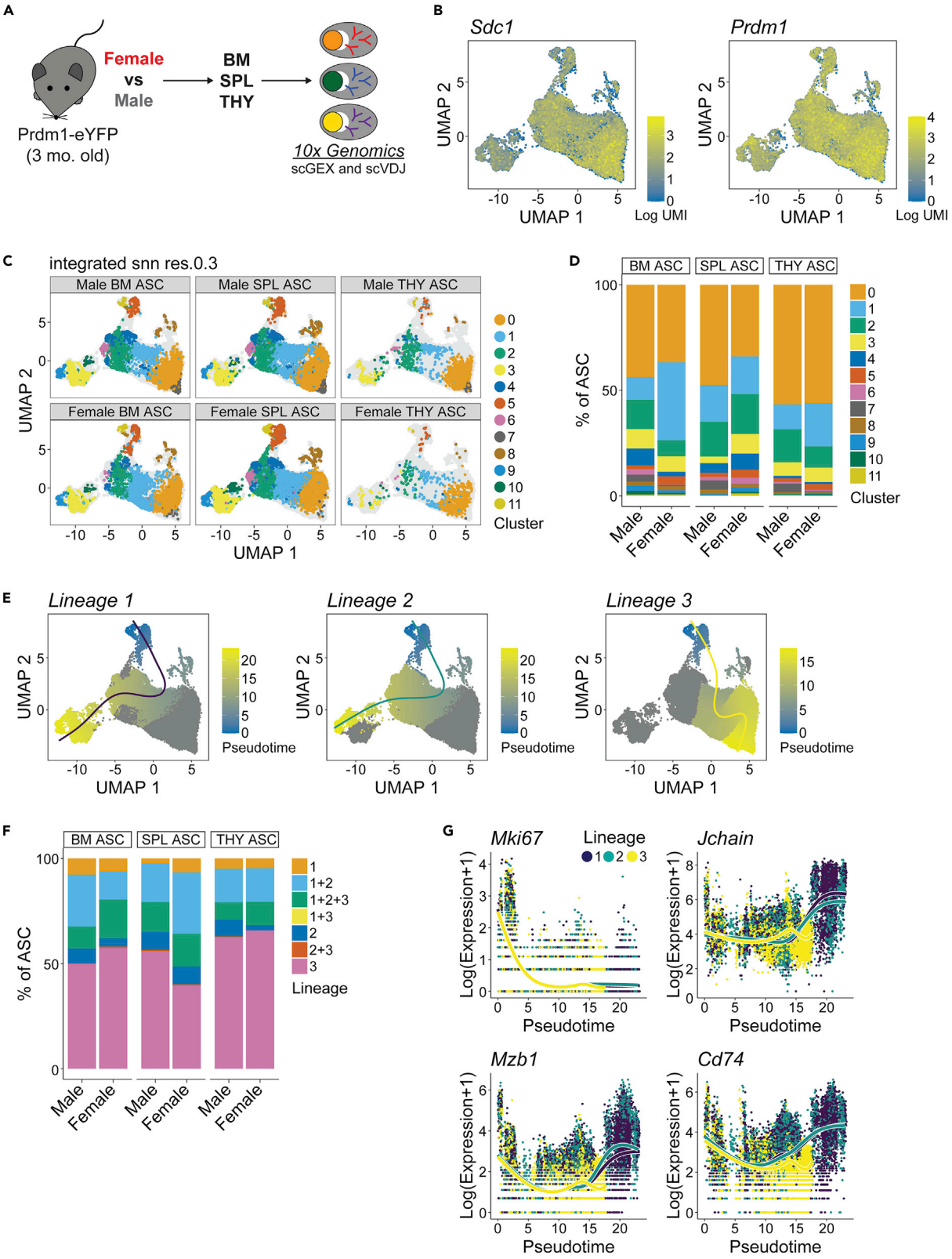
A
Female
vs
Male
BM
SPL
THY
Prdm1-eYFP
(3 mo. old)
10x Genomics
scGEX and scVDJ
B
Sdc1
Prdm1
UMAP 2
UMAP 1
Log UMI
C
integrated snn res.0.3
Male BM ASC
Male SPL ASC
Male THY ASC
Female BM ASC
Female SPL ASC
Female THY ASC
Cluster
D
BM ASC
SPL ASC
THY ASC
% of ASC
Male
Female
E
Lineage 1
Lineage 2
Lineage 3
Pseudotime
F
Lineage
G
Mki67
Jchain
Mzb1
Cd74
Log(Expression+1)
Pseudotime

Figure 5. Single cell RNA sequencing identifies antibody-secreting cell clusters and divergent lineages that exist in bone marrow, spleen and thymus, related to Figures S4 and S5, Tables S1 and S2

(A) Schematic of scRNA-seq analysis of ASCs from female and male BM, SPL and THY. Subsequent data derived from pools of 3 female and 3 male mice, respectively.

(B) UMAP plots showing log-normalized unique molecular identifier (UMI) counts for *Sdc1* and *Prdm1*.

(C) UMAP plots showing single ASCs and cluster assignments from female and male BM, SPL and THY.

(D) Graph depicting relative cluster contribution to ASC pools from female and male BM, SPL and THY.

(E) Pseudotime plots showing 3 ASC lineages.

(F) Relative contributions of various pseudotime lineages to male and female ASCs from BM, SPL and THY.

(G) Plots illustrating changes in Log(Expression+1) of *Mki67*, *Jchain*, *Mzb1* and *Cd74* over the course of pseudotime. Individual symbols depict single cells within a particular lineage.

To further assess non-Ig cluster marker genes, Metascape[54] was used to identify gene ontology (GO) associations (Table S2). We focused on GO Biological Processes and only considered terms which possessed a gene overlap of $\geq$10. We identified multiple instances where clusters shared a degree of similarity (Figures S4C–S4H). Clusters 0, 3, 8, 9 and 11 shared enrichment for protein-related biological processes such as cytoplasmic translation (GO:0002181) and those related to ribosome production (GO:0022613, GO:0042254, GO:0042255) (Figure S4C and Table S2). Metabolic biological processes were enriched in many clusters (Figure S4D and Table S2) and included terms such as oxidative phosphorylation (GO:0006119) and ATP usage/metabolism (GO:0042775, GO:0046034) which was in agreement with what is known regarding ASC metabolism.[55–57] In addition, multiple clusters (Clusters 1–2, 4–6) were enriched for events related to RNA processing (Figure S4F) and chromatin organization (GO:0006325) (Figure S4G). However, GO analysis identified some distinguishing features. Clusters 5 and 11 were enriched for terms related to the mitotic cell cycle (GO:0000278) (Figure S4E) whereas Clusters 2 and 8 were correlated with immune processes such as antigen processing and presentation (GO:0019882, GO:0048002) and/or myeloid cell homeostasis (GO:0002262) (Figure S4H). Many of the clusters and associated ontologies that we observed shared commonality with earlier single-cell ASC studies[56] lending validity to our analyses. However, our analyses suggest that ASC clusters exist with distinct functions such as those related to immune regulation.

ASCs are a composite of divergent lineages which display organ-specific changes in gene expression

The above analyses suggested some fundamental differences existed between ASC clusters. In some instances, these differences were related to UMAP position. A prime example was Clusters 0-1 and 7-8 that possessed a high percentage of Ig marker genes relative to other clusters and were segregated on the right portion of the UMAP plots (Figure 5C). This suggested that ASCs might have divergent lineages or "fates". To investigate this, we performed pseudotime analysis using the *tradeSeq* package.[58] Lineages were rooted (pseudotime = 0) at Cluster 11 based on its gene ontology association with mitosis (Figure S4E and Table S2) and high expression of cell cycle genes such as *Ccna2* (Figure S4I). Pseudotime analysis revealed 3 lineages with Lineages 1 and 2 being the most similar whereas Lineage 3 was divergent (Figure 5E). Not surprisingly, THY ASCs from both female and male mice possessed the greatest percentage of Lineage 3 "only" cells as Lineage 3 contained a large proportion of Cluster 0 (Figure 5F). For all lineages, proliferation genes such as *Mki67* (Figure 5G) showed a decrease over pseudotime. Lineages 1 and 2 demonstrated increased expression of key ASC regulatory genes such as *Jchain*,[59] *Mzb1*[60,61] and *Cd74*[62] by the termination of pseudotime (Figure 5G). In contrast, Lineage 3 showed no such increase (Figure 5G). This pattern of gene expression was pervasive amongst the lineages (Figures S5A–S5C) and perhaps indicative of the fate of Lineages 1 and 2 being that of a mature, long-lived PC rather than Lineage 3 which may be destined for a short lifespan. In agreement, Lineage 3 displayed downregulation of *Birc5* (Figure S5C) which encodes for Survivin, a key regulator of multiple myeloma growth and survival.[63,64] Of note, the gene most highly associated with Lineage 3 and that displayed increased expression over pseudotime was the long non-coding RNA (lncRNA), *Gm42418* (Figure S5C). This lncRNA has been shown to associate with the NLRP3 inflammasome in macrophages following stimulation with lipopolysaccharide and nigericin.[65] Taken together, these data support the divergence of multiple ASCs lineages whose relative percentages may be dictated in part by tissue of residence.

ASCs display sex- and organ-specific differences in VDJ repertoire

Previous studies in BM and SPL from unimmunized C57BL/6J mice demonstrated that IgM was the dominant ASC isotype in both organs.[17] To test this in THY, we performed flow cytometry for membrane IgM

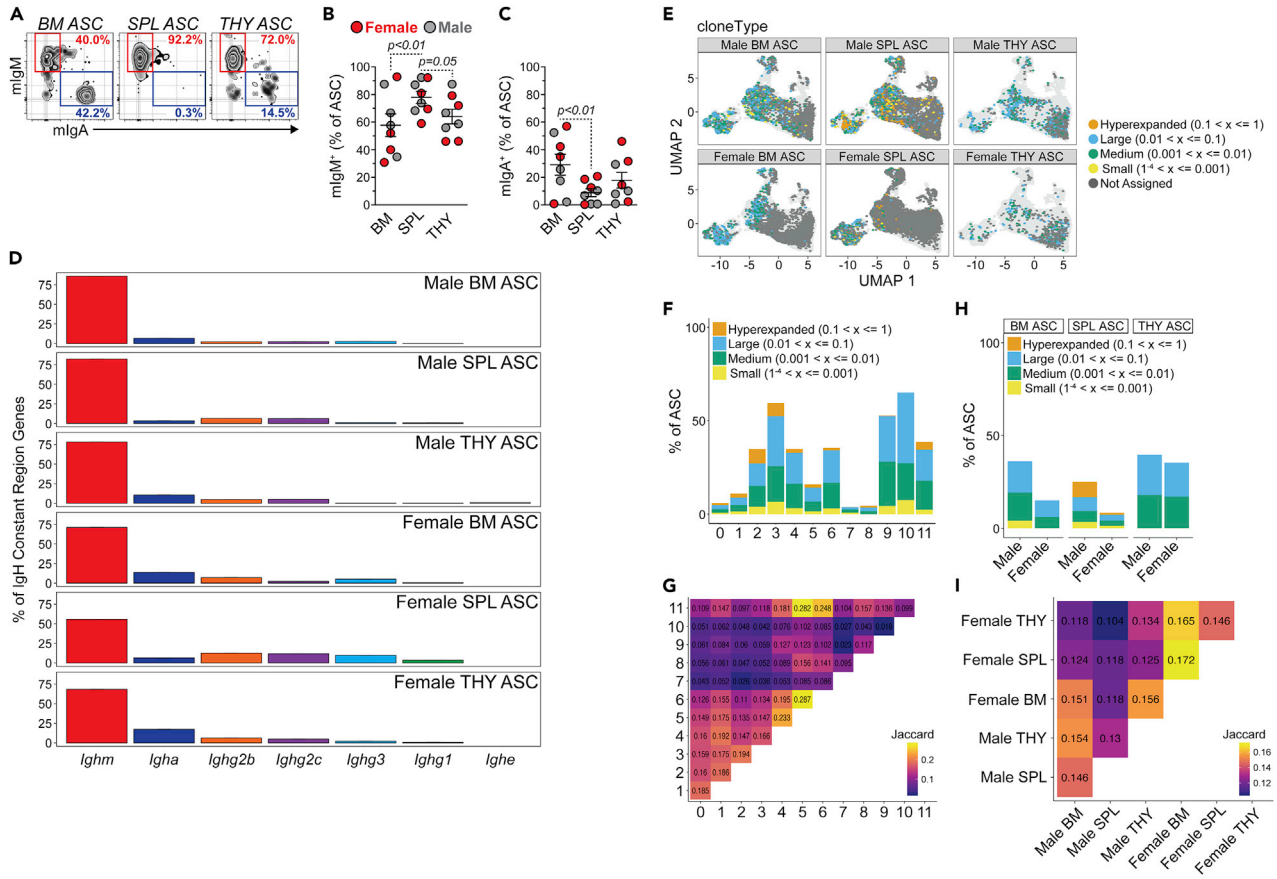

Figure 6. Antibody-secreting cell immunoglobulin repertories can be distinguished by both sex and organ

(A) Flow cytometry plots depicting representative mIgM and mIgA staining of BM, SPL and THY ASCs. Numbers in plots represent percentages within ASCs.

(B and C) Percentages of (B) mIgM$^+$ and (C) mIgA$^+$ cells with BM, SPL and THY ASCs. Symbols represent individual mice. Horizontal lines represent mean ± SEM. One-way ANOVA with Tukey's correction. Female: n = 4; Male: n = 4.

(D) Percentage of IgH constant region gene usage from female and male BM, SPL and THY ASC scRNA-seq VDJ-enriched libraries.

(E) Individual ASCs with high confidence Ig contigs overlaid on cluster UMAPs from Figure 5C. Colors correspond to clone size.

(F) Percentages of ASCs per cluster with high confidence Ig contigs as well as distribution of clone sizes within individual clusters.

(G) Plot of Jaccard indices comparing similarities between repertoires from each cluster.

(H) Percentages of ASCs per sex and organ with high confidence Ig contigs as well as distribution of clone sizes within each sample.

(I) Plot of Jaccard indices comparing similarities between repertoires from each sex and organ.

(mIgM) versus membrane IgA (mIgA) staining of ASCs from 3-mo.-old Prdm1-eYFP similar to published reports.[17,38] mIgM and mIgA expressing ASCs were observed in BM, SPL and THY (Figure 6A). SPL and THY ASCs possessed significantly higher percentages of mIgM$^+$ cells when compared to BM ASCs (Figure 6B). In contrast, BM ASCs had a higher level of mIgA positivity, at least relative to SPL (Figure 6C). Analysis of isotype usage within our 10x Genomics VDJ-enriched libraries further confirmed that IgM (coded by *Ighm*) was the dominant isotype expressed by ASCs from female and male BM, SPL and THY (Figure 6D). All 3 organs demonstrated clear isotype switching to IgA as well as the various IgG isotypes. In contrast with recent studies in BALB/c mice,[26] we did not observe a high amount of IgE (*Ighe*) expressing ASCs in the THY which may simply be due to strain differences[66,67] or animal housing.[68]

Next, we wanted to better understand how sex and organ could influence the ASC immunoglobulin repertoire. To that end, high confidence contigs were generated and clonotypes were identified based on Ig gene usage and complementarity-determining region (CDR) 3 nucleotide sequences using scRepertoire.[69] Clonotypes were merged with the scGEX data and overlaid onto cluster UMAP plots (Figure 6E) from Figure 5C. Of cells with assigned clonotypes, BM and SPL ASCs possessed a bias toward representation from the left side of the UMAP which contained Clusters 2–6 and 9–11 whereas THY ASCs had the best overall representation across their total

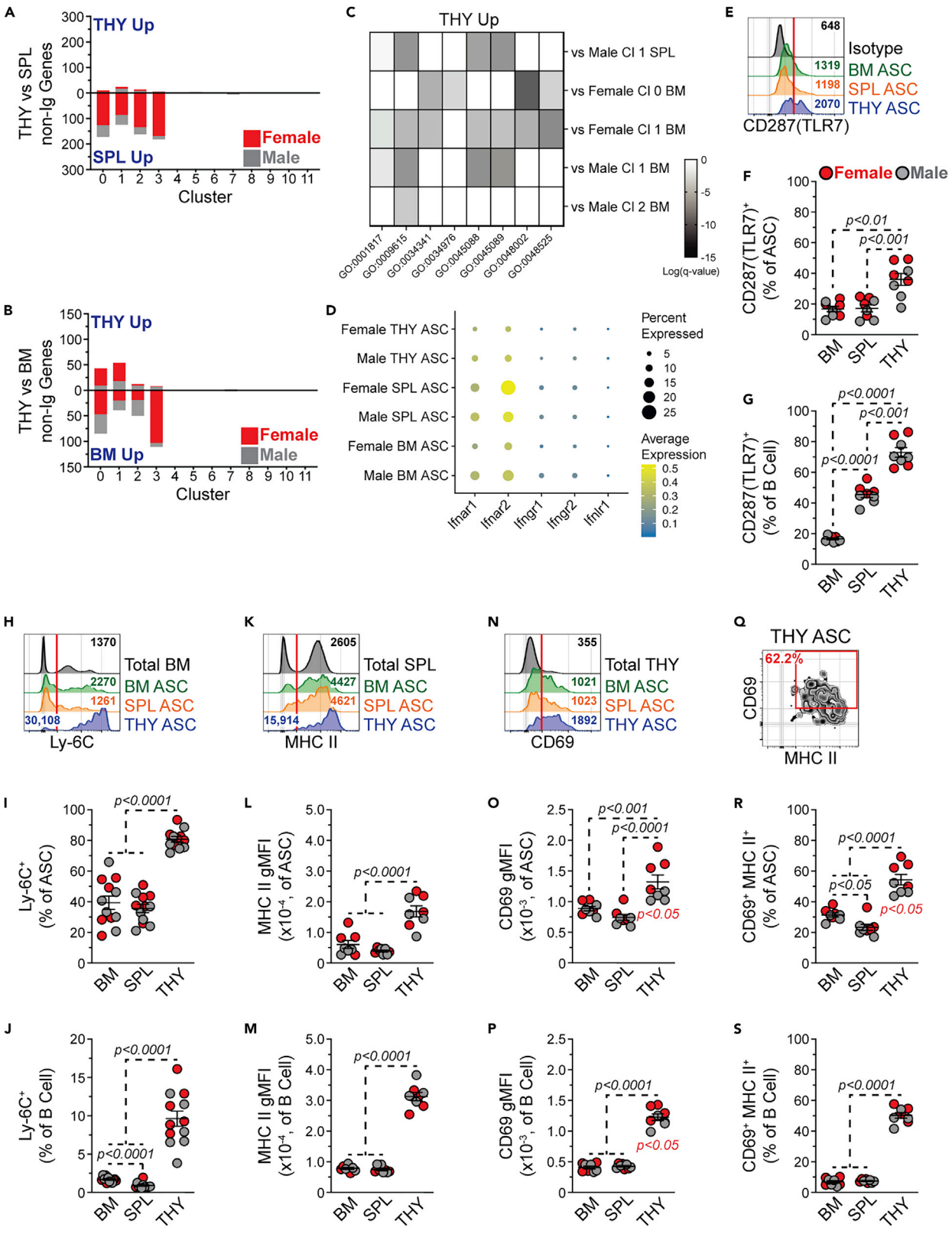
A
THY Up
SPL Up
THY vs SPL non-Ig Genes
Female
Male
Cluster
B
THY Up
BM Up
THY vs BM non-Ig Genes
Female
Male
Cluster
C
THY Up
vs Male Cl 1 SPL
vs Female Cl 0 BM
vs Female Cl 1 BM
vs Male Cl 1 BM
vs Male Cl 2 BM
GO:0001817
GO:0009615
GO:0034341
GO:0034976
GO:0045088
GO:0045089
GO:0048002
GO:0048525
Log(q-value)
D
Female THY ASC
Male THY ASC
Female SPL ASC
Male SPL ASC
Female BM ASC
Male BM ASC
Ifnar1
Ifnar2
Ifngr1
Ifngr2
Ifnlr1
Percent Expressed
Average Expression
E
Isotype
BM ASC
SPL ASC
THY ASC
CD287(TLR7)
F
Female
Male
CD287(TLR7)+ (% of ASC)
p<0.01
p<0.001
G
CD287(TLR7)+ (% of B Cell)
p<0.0001
p<0.001
p<0.0001
H
Total BM
BM ASC
SPL ASC
THY ASC
Ly-6C
I
Ly-6C+ (% of ASC)
p<0.0001
J
Ly-6C+ (% of B Cell)
p<0.0001
p<0.0001
K
Total SPL
BM ASC
SPL ASC
THY ASC
MHC II
L
MHC II gMFI (x10-4, of ASC)
p<0.0001
M
MHC II gMFI (x10-4, of B Cell)
p<0.0001
N
Total THY
BM ASC
SPL ASC
THY ASC
CD69
O
CD69 gMFI (x10-3, of ASC)
p<0.001
p<0.0001
p<0.05
P
CD69 gMFI (x10-3, of B Cell)
p<0.0001
p<0.05
Q
THY ASC
62.2%
CD69
MHC II
R
CD69+ MHC II+ (% of ASC)
p<0.0001
p<0.05
p<0.05
S
CD69+ MHC II+ (% of B Cell)
p<0.0001
BM
SPL
THY

Figure 7. Thymus antibody-secreting cells possess transcriptional and protein indicators of interferon responsiveness, related to Figures S6 and S7, Tables S3, S4, S5, S6, and S7

(A and B) Number of differentially expressed non-Ig genes in ASCs from (A) THY versus SPL and (B) THY versus BM. Data shown for females and males for all clusters.

(C) Heatmap depicting Log(q-value) statistical significance for selected GO categories associated with THY clusters whose gene expression increased relative to BM and/or SPL. Values derived from Metascape analyses presented in Tables S6 and S7.

(D) Dot plot showing average expression of log-normalized counts and percentage of cells expressing *Ifnar1*, *Ifnar2*, *Ifngr1*, *Ifngr2* and *Ifnlr1* from female and male BM, SPL and THY ASCs.

(E) Representative flow cytometry histograms depicting intracellular CD287(TLR7) staining of BM, SPL and THY ASCs. Isotype control staining of BM ASCs is shown for comparison. Red vertical line added to show cut-off for positive staining. Numbers in plots indicate gMFI.

(F and G) Percentages of CD287(TLR7)$^{+}$ cells within (F) ASCs and (G) CD45R(B220)$^{+}$ CD19^{+} CD138$^{-/LO}$ B cells from BM, SPL and THY.

(H) Representative flow cytometry histograms depicting Ly-6C surface staining of BM, SPL and THY ASCs. Total BM is shown for comparison. Red vertical line added to show cut-off for positive staining. Numbers in plots indicate gMFI.

(I and J) Percentages of Ly-6C^{+} cells within (I) ASCs and (J) CD45R(B220)$^{+}$ CD19^{+} CD138$^{-/LO}$ B cells from BM, SPL and THY.

(K) Representative flow cytometry histograms depicting MHC II surface staining of BM, SPL and THY ASCs. Total SPL is shown for comparison. Red vertical line added to show cut-off for positive staining. Numbers in plots indicate gMFI.

(L and M) MHC II gMFIs of (L) ASCs and (M) CD45R(B220)$^{+}$ CD19^{+} CD138$^{-/LO}$ B cells from BM, SPL and THY.

(N) Representative flow cytometry histograms depicting CD69 surface staining of BM, SPL and THY ASCs. Total THY is shown for comparison. Red vertical line added to show cut-off for positive staining. Numbers in plots indicate gMFI.

(O and P) CD69 gMFIs of (O) ASCs and (P) CD45R(B220)$^{+}$ CD19^{+} CD138$^{-/LO}$ B cells from BM, SPL and THY.

(Q) Representative flow cytometry plot depicting CD69 and MHC II dual surface staining on THY ASCs.

(R and S) Percentages of CD69^{+} MHC II^{+} cells within (R) ASCs and (S) CD45R(B220)$^{+}$ CD19^{+} CD138$^{-/LO}$ B cells from BM, SPL and THY.

(F, G, I, J, L, M, O, P, R and S) Symbols represent individual mice. Horizontal lines represent mean ± SEM. Unpaired Student's t-test for comparisons within sex indicated by red p values. One-way ANOVA with Tukey's correction for comparisons between organs. Female: n = 4; Male: n = 4.

clusters (Figure 6E). Examination of the data showed that clusters were differentially represented in our VDJ dataset (Figure 6F). For example, Clusters 3 and 9-10 demonstrated >50% detection of high confidence VDJ contigs within their respective ASC pools which contrasted with Clusters 0 and 7-8 which had the least representation. Many of the clusters showed evidence of clonal expansion (i.e., hyperexpanded clones ($0.1 < x \leq 1$)) which was not an artifact of depth of clonal detection/assignment as detection of hyperexpanded clones was not dependent on percentages of ASCs with VDJ contigs per cluster (Figure 6F). We next assessed clonal similarity between clusters using the Jaccard similarity index (Figure 6G) in which higher numbers represented higher similarity. Overall, clusters appeared to be clonally distinct from one another regardless of similarity in UMAP space and depth of analysis (e.g., Clusters 3 and 9-10) (Figures 5C and 6F). In this instance, Cluster 3 had similarity indices to Clusters 9 and 10 of 0.059 and 0.042, respectively (Figure 6G), whereas Clusters 9 and 10 had a similarity index of 0.018. For comparison, Clusters 5 and 6 demonstrated the highest similarity with a score of 0.287 (Figure 6G) on a scale from 0 to 1.

Finally, we examined clonality based on sample (i.e., organ and sex) (Figures 6H and 6I). Variability in clonal sizes was observed when female and male ASCs were compared in either the BM or SPL. However, this may have in part been because of the higher clonotype representation in the male BM and SPL versus the female samples (Figure 6H). Within the THY, ASC clone sizes were mostly medium ($0.001 < x \leq 0.01$) to large ($0.01 < x \leq 0.1$) and consistent across sexes (Figure 6H). Similar to what was observed for clusters, there was minimal overlap between samples when organs from a particular sex were evaluated (Figure 6I). For example, the male THY demonstrated similarity scores of 0.154 and 0.130 when compared to male BM and SPL, respectively. In addition, similarity was low between sexes. This was on display for all three organs as female versus male BM, SPL and THY had Jaccard indices of 0.151, 0.118 and 0.134 (Figure 6I). Overall, these data imply that the clonal repertoire of ASCs is dictated by the tissue of residence as well as by the sex in which those cells develop.

THY ASCs possess an interferon responsive gene expression signature

Our data showed that organ site could influence ASC lineage composition and repertoire. To further evaluate organ-specific differences, we examined gene expression changes within clusters as determined by organ (e.g., THY versus SPL) using a Log_2 Fold Change > |0.5| and an Adjusted p value <0.05 as cut-offs for significance (Tables S3, S4, and S5). When comparing THY clusters to those from the SPL (Figure 7A and Table S3) and BM (Figure 7B and Table S4), most gene changes were present as downregulated in the THY. This was primarily limited to Clusters 0-3 which made up the bulk of THY ASCs. To put these gene changes into context, we performed GO analysis (Tables S6 and S7) as above but decreased the threshold to 5 for the number of non-Ig genes included in a category. Genes downregulated in THY ASCs versus those of the SPL (Table S6) and BM (Table S7) were enriched for categories involved in both protein production (e.g., GO:0006412, GO:0042254)

and metabolism (e.g., GO:0006119, GO:0009060). Although there was some variation between clusters and sexes, these observations were generally applicable and may indicate THY ASCs being less "fit". Although the number of genes upregulated in clusters from THY ASCs was limited, there was significant association with categories related to antigen processing and presentation of peptide antigen (GO:0048002), response to IFN-gamma (γ) (GO:0034341), regulation of innate immune response (GO:0045088) and response to virus (GO:0009615) among others (Figure 7C, Tables S6 and S7). Most of these categories showed overlap of genes which included *Tlr7*, *Irf7* and a variety of IFN-stimulated genes (e.g., *Isg15*). Examination of IFN receptor gene expression suggested that Type I IFN receptor genes *Ifnar1* and *Ifnar2* were the primary receptors expressed by ASCs; however, a small percentage of cells possessed transcripts for *Ifngr1*, *Ifngr2* and *Ifnlr1* (Figure 7D).

To confirm some of these findings, we performed intracellular flow cytometry on BM, SPL and THY ASCs for CD287(TLR7).[70] This target was chosen in part because of its role in suppressing the reactivation of endogenous retroviruses which can lead to the development of T cell acute lymphoblastic leukemia (T-ALL)[71] as well as its functional link to autoimmune disease development.[72,73] CD287(TLR7) was detectable in ASCs from all 3 organs (Figure 7E). However, THY ASCs demonstrated the highest percentage of CD287(TLR7)$^+$ cells (Figure 7F). Total THY B cells also displayed an increased percentage of CD287(TLR7)$^+$ cells relative to those from BM and SPL (Figure 7G). Our gene ontology analysis suggested that THY ASC clusters possessed an IFN-inducible, or related, gene signature which was not surprising because CD287(TLR7) stimulation can induce IFN production.[74] As such, we consistently observed increased expression of *Ly6c2* in THY ASC clusters relative to other organs (Tables S3 and S4). The *Ly6c2* gene product is part of the Ly-6C cell surface complex which can be induced by both Type I and Type II IFNs.[75,76] In agreement with our scRNA-seq data, Ly-6C expression was significantly increased on the surface of THY ASCs (Figures 7H and 7I) as ~81% of THY ASCs were Ly-6C$^+$ compared to ~39% and 36% of BM and SPL ASCs, respectively (Figure 7I). Although only ~10% of THY B cells expressed Ly-6C, this was still increased over those from the BM and SPL (Figure 7J). IFN-γ signaling can also induce expression of major histocompatibility complex class II (MHC II)[77] and at least in females, we observed increased gene expression of *H2-Ab1* and *H2-Eb1* from THY Clusters 0 and 1 compared to those from the BM. Using an Ab that recognizes I-A/I-E (MHC II), we performed flow cytometry which revealed the highest MHC II surface expression on ASCs from THY (Figures 7K and 7L). This was not unique to ASCs as THY B cells possessed a similar phenotype (Figure 7M) as previously reported.[47] In addition, THY ASCs displayed increased expression of cell surface CD69 which can also be induced by IFNs[78] (Figures 7N and 7O). In agreement with earlier studies,[46] THY B cells also possessed increased CD69 levels (Figure 7P). Further evaluation of CD69 and MHC II showed a pattern of co-expression on the surface of THY ASCs (Figure 7Q). Compared to those from BM and SPL, both THY ASCs (Figure 7R) and B cells (Figure 7S) had increased percentages of CD69$^+$ MHC II$^+$ cells. Taken together, these data indicate that our scRNA-seq dataset can be leveraged to identify THY ASC phenotypes related to various cell signaling/stimulatory events.

Age-associated accumulation of THY ASCs is sex dependent

Aging in mice has been associated with the accumulation of ASCs in tissues such as BM and SPL.[13,17,79] Furthermore, ELISpot data from humans is indicative of increased ASCs in the THY with age.[23] To determine if percentages and/or numbers of mouse THY ASCs fluctuate with age, we performed flow cytometry on THY from middle-age (12-mo.-old) Prdm1-eYFP mice and compared these results to our 3-mo.-old dataset (Figures S6A–S6D). As controls for age-associated ASC accumulation, we also assessed BM and SPL (Figures S6E–S6J). As expected, THY cellularity decreased with age (Figure S6B) and this was accompanied by increased ASC percentages in the THY of both sexes (Figure S6C). However, male THY demonstrated increased numbers of ASCs with age that was not apparent in females (Figure S6D). Notably, percentages and numbers of ASCs increased in the BM and SPL with age for both sexes (Figures S6F, S6G, S6I, and S6J) with SPL ASCs having accumulated to a greater degree in females.

RNA-seq of young and old BM PCs previously identified age-associated transcriptional changes which included increased TLR expression.[17] As such, we were curious as to whether some of the organ specific ASC (and B cell) phenotypes identified above would be maintained in middle-age 12-mo.-old mice (Figures S7A–S7O). THY ASCs from middle-aged mice maintained increased CD287(TLR7) (Figures S7A and S7B), Ly-6C (Figures S7D and S7E) and MHC II (Figures S7G and S7H) levels relative to ASCs from BM and SPL. Regarding Ly-6C, female ASCs from SPL and THY displayed higher expression relative to males, although the sample number was relatively low (Figure S7E). In contrast, CD69 was no longer upregulated by THY ASCs (Figures S7J and S7K) and was downregulated in female THY ASCs relative to males.

As a result, THY ASCs were not enriched for a CD69$^+$ MHC II$^+$ population when compared to BM and SPL (Figures S7M and S7N). In comparison, expression differences identified in young THY B cells were maintained in middle-age (Figures S7C, S7F, S7I, S7L, and S7O). Of note, total B cells from a 12-mo.-old female SPL displayed increased CD287(TLR7) positivity relative to males. This was similar to that observed for female and male age-associated B cells from the DEF6:SWAP-70 double knockout lupus mouse model.[80] Collectively, these results suggest that aging impacts the THY ASC compartment and that this is at least partially sex dependent. Furthermore, these data indicate that not all THY B lineage cells age equivalently.

DISCUSSION

In this study, we provide a comprehensive resource which compares female and male ASCs found in the THY to their counterparts in organs such as the BM and SPL. From these comparisons, we identified characteristics that set THY ASCs apart and may lend themselves to unique cellular functions and regulatory mechanisms.

Initial assessment of ASC production demonstrated higher ASC numbers in young female mice relative to males. However, this sex-bias was limited to the THY and disappeared by middle-age as a result of selective ASC expansion in the male THY whereas ASC numbers remained static in the aging female THY. These data may be indicative of an upper limit of THY ASC carrying capacity which at least in females can be reached early in age. In contrast, BM and SPL demonstrated age-associated expansion of ASCs in both sexes. The surrounding environment is a key determinant of ASC accumulation and maintenance.[81] To that end, how the ASC niche evolves in aging BM and SPL may be in direct contrast to that in the THY thus ultimately limiting the carrying capacity of the THY. On face value, this could be partially explained by age-associated atrophy of the THY which would inherently limit the physical space that ASCs could occupy. For example, the THY epithelium undergoes extensive remodeling over the course of aging which includes contraction of the medullary epithelium.[82] Notably, THY B cells localize in the medullary space as do ASCs although the latter has been mostly associated with perivascular spaces within the medulla.[22,23,26] In addition, neutrophils significantly increase in the aging BM and SPL[83] and these cells have been shown to promote ASC production/maintenance through B cell activating factor (BAFF) production.[84,85] Although this may explain the numerical cap on THY ASCs, it does not inherently resolve as to why the female THY has enhanced ASC production at early age. One potential explanation may be differences in sex hormones as testosterone has been shown to reduce BAFF in young male mice[86] and BAFF transgenic mice are known to possess increased number of THY B cells.[87] Of course, this implies that THY ASC populations are inherently more susceptible to fluctuations in locally available survival factors which is something that remains to be determined.

A major question exists as to how and where THY ASCs are generated. A recent study performed histopathology, i.v. Ab labeling and long-term parabiosis experiments in BALB/c mice to support the intrathymic generation of ASCs.[26] In addition, data from humans lend further evidence for the local generation of THY ASCs.[22] We performed similar i.v. labeling experiments which confirmed observations in BALB/c mice and our analysis of THY live cell doublets identified putative B cell-T cell conjugates with enhanced levels of activation markers. Furthermore, we demonstrated the presence of proliferating (i.e., Ki-67$^+$) THY B cells and PBs which were significantly reduced on Ab-mediated blockade of CD154(CD40L) signals. Notably, magnitude differences were evident between experiments performed with Prdm1-eYFP and C57BL/6J mice. This may have been a result of different compositions within the ASC compartments (e.g., Ki-67$^+$ PBs) as these studies were performed with different strains, age-matched littermates (Prdm1-eYFP) versus not (C57BL/6J) and in different institutions. Regardless, the data indicated that at least a portion of THY ASCs were generated in a T cell dependent manner which agreed with T cell receptor (TCR) transgenic experiments performed with BALB/c mice.[26] Even though CD154 signals contributed to THY ASC generation/maintenance, we were not able to transiently augment their numbers on αCD40 stimulation *in vivo* which contrasted with what we observed in the SPL. This may be a result of different activation/signaling requirements which would agree with previous *in vitro* studies comparing activation stimuli of THY and SPL B cells.[88,89] In addition, these data could also argue for the local generation of THY ASCs as we did not observe a clear "spillover" from the peripheral SPL into the THY. This presumably would have been observable in the male THY which had lower ASC numbers at young age. Of course, we cannot rule out the potential influence on ASCs of THY gating mechanisms which are known to temporally regulate the entry of THY progenitors.[90] To do so would require experiments such as the transfer of ASC-depleted THY tissue into μMT B cell deficient mice. This would then allow for the examination of ASC production from pre-existing THY B cells without the potential caveat of immigrating B cells and/or ASCs.

ASCs continue to gain prominence as an immunomodulatory population due in part to their ability to secrete immunosuppressive as well as inflammatory factors.[9–11] In addition, this same secretory ability may influence their potential to regulate BM hematopoiesis.[16,17] As a result, understanding ASC biology is of growing importance as the repertoire of ASC functions seems to depend on the context in which ASCs exist. Along these lines, recent studies have utilized RNA-seq at both bulk[13,17,91,92] and single cell[56,93] levels in an attempt to define different ASC subsets or functional states. In general, these datasets have provided valuable resources that have led to the determination of critical ASC regulatory mechanisms. In this report, we compared ASCs from the female and male BM, SPL and THY using scRNA-seq. Our data were not only confirmatory to previous studies[56] but also provided unique insights into THY ASCs and illustrated their divergence from their BM and SPL counterparts. Via analysis of developmental trajectory (i.e., pseudotime), we defined 3 ASC lineages with the third of these appearing destined for a shorter lifespan as exemplified by reduced expression of genes related to ASC function (e.g., *Jchain*, *Mzb1*, *Cd74*) and survival (e.g., *Birc5*). In conjunction with previous studies,[25,47,94] our data supported the derivation of THY ASCs from potentially autoreactive THY B cells. As such, it is preferential that THY ASCs were enriched for Lineage 3 as this may be an evolutionary failsafe to prevent the long-standing presence of autoreactive ASCs. In this regard, it would be interesting to transcriptionally profile THY resident autoreactive ASCs that exist in diseases such as myasthenia gravis.[18] Would their gene signature resemble that of Lineages 1 and 2 rather than Lineage 3?

Regarding the potential function(s) for THY ASCs, our transcriptional profiling revealed significant anti-viral and IFN gene ontology enrichment within genes specifically upregulated in THY ASC clusters. This included genes that code for protein products including TLR7, Ly-6C and MHC II, the latter being a key factor in antigen presentation. Accordingly, flow cytometry demonstrated immunoglobulin staining on the surface of THY ASCs making it reasonable to hypothesize that autoreactive ASCs could internalize self-antigen in the THY microenvironment and present that same self-antigen to selecting T cells, thus playing a role previously attributed to total THY B cells.[25,47,94] There is precedent for this behavior as ASCs in the LN have been shown to present antigen to T follicular helper cells and suppress their behavior following model antigen immunization.[62] This would explain the minimal overlap of immunoglobulin clonotypes in THY ASCs compared to those in the BM and SPL. Previous work has demonstrated that some THY ASC-derived Abs are specific for viral and bacterial antigens; however, these data are far from comprehensive. Thus, the generation of autoreactive THY ASCs under normal conditions, regardless of their longevity, remains a distinct possibility and is in agreement with previous data in which autoreactive THY B cells in mice present antigen to negatively selecting CD4 single positive T cells.[25,47] However, comparison of THY TCR repertoires and autoreactivity in ASC wildtype and knockout mice is needed to further support a role for ASCs in thymocyte selection. Alternatively, the same TCR comparisons performed in animals in which ASCs lack components of the antigen presentation machinery (e.g., MHC II) would provide a pathway specific analysis. If this hypothesis is true, the sex bias in early life THY ASC numbers may contribute to the phenotypic and functional differences observed in T cells from females and males.[95]

In considering how the THY environment may shape resident ASC function, an open question is the potential source of IFN-inducing pathogen associated molecular patterns as well as the cellular sources of IFN in the THY. Endogenous retroviruses (ERVs) can be found in both the human[96] and mouse[71] THY and intact TLR signaling, in particularly TLR7, is critical in preventing reactivation of these ERVs.[71] As TLR7 signaling is a potent inducer of Type I IFN, this regulatory loop would explain the constitutive IFN-α expression in the human THY.[97] In this instance, IFN-α was produced by THY plasmacytoid dendritic cells. Given the level of TLR7 expression, one could ask if THY ASCs can themselves produce IFNs? Our data would not necessarily support this as we did not see clear IFN (e.g., *Ifnb*) induction in THY ASCs. However, this could be a consequence of single cell sequencing technologies which do not efficiently capture low expression genes,[98] thus the idea of direct TLR7-mediated IFN induction in THY ASCs warrants further investigation. Finally, is the observed IFN gene signature of THY ASCs a result of direct IFN stimulation or is this inherited from upstream B cell progenitors? Transcriptome data demonstrated Type I IFN receptor expression by at least a portion of THY ASCs raising the possibility of their direct responsiveness to this cytokine family. Combined with the above, THY ASCs may propagate their own feedforward IFN signaling loop for unknown reasons, although this remains conjecture at this point.

In summary, the data presented here support the concept that THY ASCs develop independently of their peripheral counterparts and possess a gene signature that is dictated by their local microenvironment

(e.g., IFN signaling in the THY[71]). Importantly, we have developed a comprehensive scRNA-seq data resource that can be utilized by researchers to develop testable hypotheses investigating the development, maintenance and function of THY ASCs.

Limitations of the study

The work presented here focused on the comparisons of female and male ASCs from BM, SPL and THY. This was done for multiple reasons which include: 1) Well-established roles of BM (i.e., residency) and SPL (i.e., production and residency) in ASC biology and 2) lack of tissue digestion required to analyze ASCs in all 3 organs. This latter point being important as some cell surface markers are inherently sensitive to enzymatic digestion which may inadvertently skew results. However, future studies evaluating the relatedness of gut and THY ASCs will be important. For example, plasmacytoid dendritic cells are known to transport microbial antigens from the gut to the THY thus it is plausible that these ASC populations share significant overlap in their immunoglobulin repertoires. In this sense, comparison of these populations may further elucidate how tissue residency independent of Ab reactivities may shape ASC behavior. In addition, we were not in position to perform scRNA-seq on aging THY ASCs. As bulk RNA-seq has provided clues to age-associated changes in BM plasma cell behavior,[17] a similar analysis either at bulk or single cell levels may be just as informative regarding functionality of THY ASCs.

STAR★METHODS

Detailed methods are provided in the online version of this paper and include the following:

- KEY RESOURCES TABLE
- RESOURCE AVAILABILITY
  - Lead contact
  - Materials availability
  - Data and code availability
- EXPERIMENTAL MODEL AND SUBJECT DETAILS
  - Experimental animals
- METHOD DETAILS
  - Isolation of bone marrow, spleen and thymus tissue
  - Immunostaining
  - Flow cytometry and fluorescence-activated cell sorting
  - Enzyme-linked immunosorbent spot assay
  - *In vivo* CD45 labeling
  - *In vivo*CD154(CD40L) blockade
  - *In vivo* CD40 stimulation
  - 10x genomics single cell library preparation, sequencing and analysis
- QUANTIFICATION AND STATISTICAL ANALYSIS

SUPPLEMENTAL INFORMATION

Supplemental information can be found online at https://doi.org/10.1016/j.isci.2023.106223.

ACKNOWLEDGMENTS

Funding was provided by the Western Michigan University Homer Stryker M.D. School of Medicine (WMed) and the University of Saskatchewan (USask) College of Medicine via intramural startup funds. This work was further supported by the National Institute on Aging of the National Institutes of Health under Award Number R03AG071955. The content is solely the responsibility of the authors and does not necessarily represent the official views of the National Institutes of Health. The authors thank WMed students Michael Crone, Matthew Kornas and Patrick Renner for their technical assistance. The authors thank the Van Andel Genomics Core and Bioinformatics and Biostatistics Core for providing sequencing facilities and analysis services, respectively.

AUTHOR CONTRIBUTIONS

K.T.P. and P.D.P. designed experiments. K.T.P. and P.D.P. conducted and analyzed experiments. K.H.L. performed bioinformatics analyses. P.D.P. wrote the manuscript and all authors approved of the manuscript.

DECLARATION OF INTERESTS

The authors declare no competing interests.

INCLUSION AND DIVERSITY

We support inclusive, diverse and equitable conduct of research.

Received: June 23, 2022
Revised: January 5, 2023
Accepted: February 11, 2023
Published: February 15, 2023

REFERENCES

1. Forthal, D.N. (2014). Functions of antibodies. Microbiol.Spectr. *2*. https://doi.org/10.1128/microbiolspec.AID-0019-2014.

2. Slifka, M.K., Antia, R., Whitmire, J.K., and Ahmed, R. (1998). Humoral immunity due to long-lived plasma cells. Immunity *8*, 363–372. https://doi.org/10.1016/s1074-7613(00)80541-5.

3. Chernova, I., Jones, D.D., Wilmore, J.R., Bortnick, A., Yucel, M., Hershberg, U., and Allman, D. (2014). Lasting antibody responses are mediated by a combination of newly formed and established bone marrow plasma cells drawn from clonally distinct precursors. J. Immunol. *193*, 4971–4979. https://doi.org/10.4049/jimmunol.1401264.

4. Manz, R.A., Löhning, M., Cassese, G., Thiel, A., and Radbruch, A. (1998). Survival of long-lived plasma cells is independent of antigen. Int. Immunol. *10*, 1703–1711. https://doi.org/10.1093/intimm/10.11.1703.

5. Manz, R.A., Thiel, A., and Radbruch, A. (1997). Lifetime of plasma cells in the bone marrow. Nature *388*, 133–134. https://doi.org/10.1038/40540.

6. Amanna, I.J., Carlson, N.E., and Slifka, M.K. (2007). Duration of humoral immunity to common viral and vaccine antigens. N. Engl. J. Med. *357*, 1903–1915. https://doi.org/10.1056/NEJMoa066092.

7. Halliley, J.L., Tipton, C.M., Liesveld, J., Rosenberg, A.F., Darce, J., Gregoretti, I.V., Popova, L., Kaminiski, D., Fucile, C.F., Albizua, I., et al. (2015). Long-lived plasma cells are contained within the CD19(-)CD38(hi)CD138(+) subset in human bone marrow. Immunity *43*, 132–145. https://doi.org/10.1016/j.immuni.2015.06.016.

8. Landsverk, O.J.B., Snir, O., Casado, R.B., Richter, L., Mold, J.E., Réu, P., Horneland, R., Paulsen, V., Yaqub, S., Aandahl, E.M., et al. (2017). Antibody-secreting plasma cells persist for decades in human intestine. J. Exp. Med. *214*, 309–317. https://doi.org/10.1084/jem.20161590.

9. Fillatreau, S. (2019). Regulatory functions of B cells and regulatory plasma cells. Biomed. J. *42*, 233–242. https://doi.org/10.1016/j.bj.2019.05.008.

10. Pioli, P.D. (2019). Plasma cells, the next generation: beyond antibody secretion. Front. Immunol. *10*, 2768. https://doi.org/10.3389/fimmu.2019.02768.

11. Wang, A.A., Gommerman, J.L., and Rojas, O.L. (2021). Plasma cells: from cytokine production to regulation in experimental autoimmune encephalomyelitis. J. Mol. Biol. *433*, 166655. https://doi.org/10.1016/j.jmb.2020.09.014.

12. Rojas, O.L., Pröbstel, A.K., Porfilio, E.A., Wang, A.A., Charabati, M., Sun, T., Lee, D.S.W., Galicia, G., Ramaglia, V., Ward, L.A., et al. (2019). Recirculating intestinal IgA-producing cells regulate neuroinflammation via IL-10. Cell *177*, 492–493. https://doi.org/10.1016/j.cell.2019.03.037.

13. Lino, A.C., Dang, V.D., Lampropoulou, V., Welle, A., Joedicke, J., Pohar, J., Simon, Q., Thalmensi, J., Baures, A., Flühler, V., et al. (2018). LAG-3 inhibitory receptor expression identifies immunosuppressive natural regulatory plasma cells. Immunity *49*, 120–133.e9. https://doi.org/10.1016/j.immuni.2018.06.007.

14. Fritz, J.H., Rojas, O.L., Simard, N., McCarthy, D.D., Hapfelmeier, S., Rubino, S., Robertson, S.J., Larijani, M., Gosselin, J., Ivanov, I.I., et al. (2011). Acquisition of a multifunctional IgA+ plasma cell phenotype in the gut. Nature *481*, 199–203. https://doi.org/10.1038/nature10698.

15. Bermejo, D.A., Jackson, S.W., Gorosito-Serran, M., Acosta-Rodriguez, E.V., Amezcua-Vesely, M.C., Sather, B.D., Singh, A.K., Khim, S., Mucci, J., Liggitt, D., et al. (2013). Trypanosoma cruzi trans-sialidase initiates a program independent of the transcription factors RORgammat and Ahr that leads to IL-17 production by activated B cells. Nat. Immunol. *14*, 514–522. https://doi.org/10.1038/ni.2569.

16. Meng, L., Almeida, L.N., Clauder, A.K., Lindemann, T., Luther, J., Link, C., Hofmann, K., Kulkarni, U., Wong, D.M., David, J.P., and Manz, R.A. (2019). Bone marrow plasma cells modulate local myeloid-lineage differentiation via IL-10. Front. Immunol. *10*, 1183. https://doi.org/10.3389/fimmu.2019.01183.

17. Pioli, P.D., Casero, D., Montecino-Rodriguez, E., Morrison, S.L., and Dorshkind, K. (2019). Plasma cells are obligate effectors of enhanced myelopoiesis in aging bone marrow. Immunity *51*, 351–366.e6. https://doi.org/10.1016/j.immuni.2019.06.006.

18. Hill, M.E., Shiono, H., Newsom-Davis, J., and Willcox, N. (2008). The myasthenia gravis thymus: a rare source of human autoantibody-secreting plasma cells for testing potential therapeutics. J. Neuroimmunol. *201–202*, 50–56. https://doi.org/10.1016/j.jneuroim.2008.06.027.

19. Yamamoto, Y., Matsui, N., Uzawa, A., Ozawa, Y., Kanai, T., Oda, F., Kondo, H., Ohigashi, I., Takizawa, H., Kondo, K., et al. (2021). Intrathymic plasmablasts are affected in patients with myasthenia gravis with active disease. Neurol. Neuroimmunol. Neuroinflamm. *8*, e1087. https://doi.org/10.1212/NXI.0000000000001087.

20. Zografou, C., Vakrakou, A.G., and Stathopoulos, P. (2021). Short- and long-lived autoantibody-secreting cells in autoimmune neurological disorders. Front. Immunol. *12*, 686466. https://doi.org/10.3389/fimmu.2021.686466.

21. Hidalgo, Y., Núñez, S., Fuenzalida, M.J., Flores-Santibáñez, F., Sáez, P.J., Dorner, J., Lennon-Dumenil, A.M., Martínez, V., Zorn, E., Rosemblatt, M., et al. (2020). Thymic B cells promote germinal center-like structures and the expansion of follicular helper T cells in lupus-prone mice. Front. Immunol. *11*, 696. https://doi.org/10.3389/fimmu.2020.00696.

22. Cordero, H., King, R.G., Dogra, P., Dufeu, C., See, S.B., Chong, A.M., Uhlemann, A.C., Ho, S.H., Kalfa, D.M., Bacha, E.A., et al. (2021). Intrathymic differentiation of natural antibody-producing plasma cells in human neonates. Nat. Commun. *12*, 5761. https://doi.org/10.1038/s41467-021-26069-2.

23. Nuñez, S., Moore, C., Gao, B., Rogers, K., Hidalgo, Y., Del Nido, P.J., Restaino, S., Naka, Y., Bhagat, G., Madsen, J.C., et al. (2016). The human thymus perivascular space is a functional niche for viral-specific plasma cells. Sci. Immunol. *1*, eaah4447. https://doi.org/10.1126/sciimmunol.aah4447.

24. Rother, M.B., Schreurs, M.W.J., Kroek, R., Bartol, S.J.W., van Dongen, J.J.M., and van Zelm, M.C. (2016). The human thymus is enriched for autoreactive B cells.

J. Immunol. *197*, 441–448. https://doi.org/10.4049/jimmunol.1501992.

25. Perera, J., Zheng, Z., Li, S., Gudjonson, H., Kalinina, O., Benichou, J.I.C., Block, K.E., Louzoun, Y., Yin, D., Chong, A.S., et al. (2016). Self-antigen-driven thymic B cell class switching promotes T cell central tolerance. Cell Rep. *17*, 387–398. https://doi.org/10.1016/j.celrep.2016.09.011.

26. Kwon, D.I., Park, E.S., Kim, M., Choi, Y.H., Lee, M.S., Joo, S.H., Kang, Y.W., Lee, M., Jo, S.B., Lee, S.W., et al. (2022). Homeostatic serum IgE is secreted by plasma cells in the thymus and enhances mast cell survival. Nat. Commun. *13*, 1418. https://doi.org/10.1038/s41467-022-29032-x.

27. Klein, S.L., and Flanagan, K.L. (2016). Sex differences in immune responses. Nat. Rev. Immunol. *16*, 626–638. https://doi.org/10.1038/nri.2016.90.

28. Haba, S., and Nisonoff, A. (1992). IgE-secreting cells in the thymus: correlation with induction of tolerance to IgE. Proc. Natl. Acad. Sci. USA *89*, 5185–5187. https://doi.org/10.1073/pnas.89.11.5185.

29. Fooksman, D.R., Nussenzweig, M.C., and Dustin, M.L. (2014). Myeloid cells limit production of antibody-secreting cells after immunization in the lymph node. J. Immunol. *192*, 1004–1012. https://doi.org/10.4049/jimmunol.1300977.

30. Gui, J., Morales, A.J., Maxey, S.E., Bessette, K.A., Ratcliffe, N.R., Kelly, J.A., and Craig, R.W. (2011). MCL1 increases primitive thymocyte viability in female mice and promotes thymic expansion into adulthood. Int. Immunol. *23*, 647–659. https://doi.org/10.1093/intimm/dxr073.

31. Min, H., Montecino-Rodriguez, E., and Dorshkind, K. (2006). Reassessing the role of growth hormone and sex steroids in thymic involution. Clin.Immunol. *118*, 117–123. https://doi.org/10.1016/j.clim.2005.08.015.

32. Cheng, Q., Pelz, A., Taddeo, A., Khodadadi, L., Klotsche, J., Hoyer, B.F., Alexander, T., Thiel, A., Burmester, G.R., Radbruch, A., and Hiepe, F. (2020). Selective depletion of plasma cells in vivo based on the specificity of their secreted antibodies. Eur. J. Immunol. *50*, 284–291. https://doi.org/10.1002/eji.201948144.

33. Shen, P., Roch, T., Lampropoulou, V., O'Connor, R.A., Stervbo, U., Hilgenberg, E., Ries, S., Dang, V.D., Jaimes, Y., Daridon, C., et al. (2014). IL-35-producing B cells are critical regulators of immunity during autoimmune and infectious diseases. Nature *507*, 366–370. https://doi.org/10.1038/nature12979.

34. Matsumoto, M., Baba, A., Yokota, T., Nishikawa, H., Ohkawa, Y., Kayama, H., Kallies, A., Nutt, S.L., Sakaguchi, S., Takeda, K., et al. (2014). Interleukin-10-producing plasmablasts exert regulatory function in autoimmune inflammation. Immunity *41*, 1040–1051. https://doi.org/10.1016/j.immuni.2014.10.016.

35. Suzuki-Yamazaki, N., Yanobu-Takanashi, R., Okamura, T., and Takaki, S. (2017). IL-10 production in murine IgM(+) CD138(hi) cells is driven by Blimp-1 and downregulated in class-switched cells. Eur. J. Immunol. *47*, 493–503. https://doi.org/10.1002/eji.201646549.

36. Underhill, G.H., Minges Wols, H.A., Fornek, J.L., Witte, P.L., and Kansas, G.S. (2002). IgG plasma cells display a unique spectrum of leukocyte adhesion and homing molecules. Blood *99*, 2905–2912. https://doi.org/10.1182/blood.v99.8.2905.

37. Wilmore, J.R., Jones, D.D., and Allman, D. (2017). Protocol for improved resolution of plasma cell subpopulations by flow cytometry. Eur. J. Immunol. *47*, 1386–1388. https://doi.org/10.1002/eji.201746944.

38. Blanc, P., Moro-Sibilot, L., Barthly, L., Jagot, F., This, S., de Bernard, S., Buffat, L., Dussurgey, S., Colisson, R., Hobeika, E., et al. (2016). Mature IgM-expressing plasma cells sense antigen and develop competence for cytokine production upon antigenic challenge. Nat. Commun. *7*, 13600. https://doi.org/10.1038/ncomms13600.

39. Pinto, D., Montani, E., Bolli, M., Garavaglia, G., Sallusto, F., Lanzavecchia, A., and Jarrossay, D. (2013). A functional BCR in human IgA and IgM plasma cells. Blood *121*, 4110–4114. https://doi.org/10.1182/blood-2012-09-459289.

40. Minnich, M., Tagoh, H., Bönelt, P., Axelsson, E., Fischer, M., Cebolla, B., Tarakhovsky, A., Nutt, S.L., Jaritz, M., and Busslinger, M. (2016). Multifunctional role of the transcription factor Blimp-1 in coordinating plasma cell differentiation. Nat. Immunol. *17*, 331–343. https://doi.org/10.1038/ni.3349.

41. Shaffer, A.L., Lin, K.I., Kuo, T.C., Yu, X., Hurt, E.M., Rosenwald, A., Giltnane, J.M., Yang, L., Zhao, H., Calame, K., and Staudt, L.M. (2002). Blimp-1 orchestrates plasma cell differentiation by extinguishing the mature B cell gene expression program. Immunity *17*, 51–62. https://doi.org/10.1016/s1074-7613(02)00335-7.

42. Tellier, J., Shi, W., Minnich, M., Liao, Y., Crawford, S., Smyth, G.K., Kallies, A., Busslinger, M., and Nutt, S.L. (2016). Blimp-1 controls plasma cell function through the regulation of immunoglobulin secretion and the unfolded protein response. Nat. Immunol. *17*, 323–330. https://doi.org/10.1038/ni.3348.

43. Shapiro-Shelef, M., Lin, K.I., McHeyzer-Williams, L.J., Liao, J., McHeyzer-Williams, M.G., and Calame, K. (2003). Blimp-1 is required for the formation of immunoglobulin secreting plasma cells and pre-plasma memory B cells. Immunity *19*, 607–620.

44. Hobeika, E., Thiemann, S., Storch, B., Jumaa, H., Nielsen, P.J., Pelanda, R., and Reth, M. (2006). Testing gene function early in the B cell lineage in mb1-cre mice. Proc. Natl. Acad. Sci. USA *103*, 13789–13794. https://doi.org/10.1073/pnas.0605944103.

45. Pracht, K., Meinzinger, J., Daum, P., Schulz, S.R., Reimer, D., Hauke, M., Roth, E., Mielenz, D., Berek, C., Côrte-Real, J., et al. (2017). A new staining protocol for detection of murine antibody-secreting plasma cell subsets by flow cytometry. Eur. J. Immunol. *47*, 1389–1392. https://doi.org/10.1002/eji.201747019.

46. Ferrero, I., Anjuere, F., Martin, P., Martinez del Hoyo, G., Fraga, M.L., Wright, N., Varona, R., Marquez, G., and Ardavin, C. (1999). Functional and phenotypic analysis of thymic B cells: role in the induction of T cell negative selection. Eur. J. Immunol. *29*, 1598–1609. https://doi.org/10.1002/(SICI)1521-4141.

47. Perera, J., Meng, L., Meng, F., and Huang, H. (2013). Autoreactive thymic B cells are efficient antigen-presenting cells of cognate self-antigens for T cell negative selection. Proc. Natl. Acad. Sci. USA *110*, 17011–17016. https://doi.org/10.1073/pnas.1313001110.

48. Radomir, L., Cohen, S., Kramer, M.P., Bakos, E., Lewinsky, H., Barak, A., Porat, Z., Bucala, R., Stepensky, P., Becker-Herman, S., and Shachar, I. (2017). T cells regulate peripheral naive mature B cell survival by cell-cell contact mediated through SLAMF6 and SAP. J. Immunol. *199*, 2745–2757. https://doi.org/10.4049/jimmunol.1700557.

49. Anderson, K.G., Mayer-Barber, K., Sung, H., Beura, L., James, B.R., Taylor, J.J., Qunaj, L., Griffith, T.S., Vezys, V., Barber, D.L., and Masopust, D. (2014). Intravascular staining for discrimination of vascular and tissue leukocytes. Nat. Protoc. *9*, 209–222. https://doi.org/10.1038/nprot.2014.005.

50. Ruscher, R., and Hogquist, K.A. (2018). Intravenous labeling and analysis of the content of thymic perivascular spaces. Bio.Protoc. *8*, e2757. https://doi.org/10.21769/bioprotoc.2757.

51. Thanabalasuriar, A., Neupane, A.S., Wang, J., Krummel, M.F., and Kubes, P. (2016). iNKT cell emigration out of the lung vasculature requires neutrophils and monocyte-derived dendritic cells in inflammation. Cell Rep. *16*, 3260–3272. https://doi.org/10.1016/j.celrep.2016.07.052.

52. Nutt, S.L., Hodgkin, P.D., Tarlinton, D.M., and Corcoran, L.M. (2015). The generation of antibody-secreting plasma cells. Nat. Rev. Immunol. *15*, 160–171. https://doi.org/10.1038/nri3795.

53. Scharer, C.D., Patterson, D.G., Mi, T., Price, M.J., Hicks, S.L., and Boss, J.M. (2020). Antibody-secreting cell destiny emerges during the initial stages of B-cell activation. Nat. Commun. *11*, 3989. https://doi.org/10.1038/s41467-020-17798-x.

54. Zhou, Y., Zhou, B., Pache, L., Chang, M., Khodabakhshi, A.H., Tanaseichuk, O., Benner, C., and Chanda, S.K. (2019). Metascape provides a biologist-oriented resource for the analysis of systems-level datasets. Nat. Commun. *10*, 1523. https://doi.org/10.1038/s41467-019-09234-6.

55. Lam, W.Y., Becker, A.M., Kennerly, K.M., Wong, R., Curtis, J.D., Llufrio, E.M., McCommis, K.S., Fahrmann, J., Pizzato, H.A., Nunley, R.M., et al. (2016). Mitochondrial pyruvate import promotes long-term survival of antibody-secreting plasma cells. Immunity *45*, 60–73. https://doi.org/10.1016/j.immuni.2016.06.011.

56. Lam, W.Y., Jash, A., Yao, C.H., D'Souza, L., Wong, R., Nunley, R.M., Meares, G.P., Patti, G.J., and Bhattacharya, D. (2018). Metabolic and transcriptional modules independently diversify plasma cell lifespan and function. Cell Rep. *24*, 2479–2492.e6. https://doi.org/10.1016/j.celrep.2018.07.084.

57. Price, M.J., Patterson, D.G., Scharer, C.D., and Boss, J.M. (2018). Progressive upregulation of oxidative metabolism facilitates plasmablast differentiation to a T-independent antigen. Cell Rep. *23*, 3152–3159. https://doi.org/10.1016/j.celrep.2018.05.053.

58. Van den Berge, K., Roux de Bézieux, H., Street, K., Saelens, W., Cannoodt, R., Saeys, Y., Dudoit, S., and Clement, L. (2020). Trajectory-based differential expression analysis for single-cell sequencing data. Nat. Commun. *11*, 1201. https://doi.org/10.1038/s41467-020-14766-3.

59. Hendrickson, B.A., Conner, D.A., Ladd, D.J., Kendall, D., Casanova, J.E., Corthesy, B., Max, E.E., Neutra, M.R., Seidman, C.E., and Seidman, J.G. (1995). Altered hepatic transport of immunoglobulin A in mice lacking the J chain. J. Exp. Med. *182*, 1905–1911. https://doi.org/10.1084/jem.182.6.1905.

60. Andreani, V., Ramamoorthy, S., Pandey, A., Lupar, E., Nutt, S.L., Lämmermann, T., and Grosschedl, R. (2018). Cochaperone Mzb1 is a key effector of Blimp1 in plasma cell differentiation and beta1-integrin function. Proc. Natl. Acad. Sci. USA *115*, E9630–E9639. https://doi.org/10.1073/pnas.1809739115.

61. Rosenbaum, M., Andreani, V., Kapoor, T., Herp, S., Flach, H., Duchniewicz, M., and Grosschedl, R. (2014). MZB1 is a GRP94 cochaperone that enables proper immunoglobulin heavy chain biosynthesis upon ER stress. Genes Dev. *28*, 1165–1178. https://doi.org/10.1101/gad.240762.114.

62. Pelletier, N., McHeyzer-Williams, L.J., Wong, K.A., Urich, E., Fazilleau, N., and McHeyzer-Williams, M.G. (2010). Plasma cells negatively regulate the follicular helper T cell program. Nat. Immunol. *11*, 1110–1118. https://doi.org/10.1038/ni.1954.

63. Abdi, J., Rastgoo, N., Chen, Y., Chen, G.A., and Chang, H. (2019). Ectopic expression of BIRC5-targeting miR-101-3p overcomes bone marrow stroma-mediated drug resistance in multiple myeloma cells. BMC Cancer *19*, 975. https://doi.org/10.1186/s12885-019-6151-x.

64. Romagnoli, M., Trichet, V., David, C., Clément, M., Moreau, P., Bataille, R., and Barillé-Nion, S. (2007). Significant impact of survivin on myeloma cell growth. Leukemia *21*, 1070–1078. https://doi.org/10.1038/sj.leu.2404602.

65. Zhang, P., Cao, L., Zhou, R., Yang, X., and Wu, M. (2019). The lncRNA Neat1 promotes activation of inflammasomes in macrophages. Nat. Commun. *10*, 1495. https://doi.org/10.1038/s41467-019-09482-6.

66. Morokata, T., Ishikawa, J., Ida, K., and Yamada, T. (1999). C57BL/6 mice are more susceptible to antigen-induced pulmonary eosinophilia than BALB/c mice, irrespective of systemic T helper 1/T helper 2 responses. Immunology *98*, 345–351. https://doi.org/10.1046/j.1365-2567.1999.00890.x.

67. Teufelberger, A.R., Van Nevel, S., Hulpiau, P., Nordengrün, M., Savvides, S.N., De Graeve, S., Akula, S., Holtappels, G., De Ruyck, N., Declercq, W., et al. (2020). Mouse strain-dependent difference toward the Staphylococcus aureus allergen serine protease-like protein D reveals a novel regulator of IL-33. Front. Immunol. *11*, 582044. https://doi.org/10.3389/fimmu.2020.582044.

68. Wilmore, J.R., Gaudette, B.T., Gomez Atria, D., Hashemi, T., Jones, D.D., Gardner, C.A., Cole, S.D., Misic, A.M., Beiting, D.P., and Allman, D. (2018). Commensal microbes induce serum IgA responses that protect against polymicrobial sepsis. Cell Host Microbe *23*, 302–311.e3. https://doi.org/10.1016/j.chom.2018.01.005.

69. Borcherding, N., Bormann, N.L., and Kraus, G. (2020). scRepertoire: an R-based toolkit for single-cell immune receptor analysis. F1000Res. *9*, 47. https://doi.org/10.12688/f1000research.22139.2.

70. Renner, P., Crone, M., Kornas, M., Pioli, K.T., and Pioli, P.D. (2022). Intracellular flow cytometry staining of antibody-secreting cells using phycoerythrin-conjugated antibodies: pitfalls and solutions. Antib.Ther. *5*, 151–163. https://doi.org/10.1093/abt/tbac013.

71. Yu, P., Lübben, W., Slomka, H., Gebler, J., Konert, M., Cai, C., Neubrandt, L., Prazeres da Costa, O., Paul, S., Dehnert, S., et al. (2012). Nucleic acid-sensing Toll-like receptors are essential for the control of endogenous retrovirus viremia and ERV-induced tumors. Immunity *37*, 867–879. https://doi.org/10.1016/j.immuni.2012.07.018.

72. Brown, G.J., Cañete, P.F., Wang, H., Medhavy, A., Bones, J., Roco, J.A., He, Y., Qin, Y., Cappello, J., Ellyard, J.I., et al. (2022). TLR7 gain-of-function genetic variation causes human lupus. Nature *605*, 349–356. https://doi.org/10.1038/s41586-022-04642-z.

73. Murakami, Y., Fukui, R., Tanaka, R., Motoi, Y., Kanno, A., Sato, R., Yamaguchi, K., Amano, H., Furukawa, Y., Suzuki, H., et al. (2021). Anti-TLR7 antibody protects against lupus nephritis in NZBWF1 mice by targeting B cells and patrolling monocytes. Front. Immunol. *12*, 777197. https://doi.org/10.3389/fimmu.2021.777197.

74. Saitoh, S.I., Abe, F., Kanno, A., Tanimura, N., Mori Saitoh, Y., Fukui, R., Shibata, T., Sato, K., Ichinohe, T., Hayashi, M., et al. (2017). TLR7 mediated viral recognition results in focal type I interferon secretion by dendritic cells. Nat. Commun. *8*, 1592. https://doi.org/10.1038/s41467-017-01687-x.

75. Jutila, M.A., Kroese, F.G., Jutila, K.L., Stall, A.M., Fiering, S., Herzenberg, L.A., Berg, E.L., and Butcher, E.C. (1988). Ly-6C is a monocyte/macrophage and endothelial cell differentiation antigen regulated by interferon-gamma. Eur. J. Immunol. *18*, 1819–1826. https://doi.org/10.1002/eji.1830181125.

76. Schlueter, A.J., Krieg, A.M., de Vries, P., and Li, X. (2001). Type I interferon is the primary regulator of inducible Ly-6C expression on T cells. J. Interferon Cytokine Res. *21*, 621–629. https://doi.org/10.1089/10799900152547885.

77. Collins, T., Korman, A.J., Wake, C.T., Boss, J.M., Kappes, D.J., Fiers, W., Ault, K.A., Gimbrone, M.A., Jr., Strominger, J.L., and Pober, J.S. (1984). Immune interferon activates multiple class II major histocompatibility complex genes and the associated invariant chain gene in human endothelial cells and dermal fibroblasts. Proc. Natl. Acad. Sci. USA *81*, 4917–4921. https://doi.org/10.1073/pnas.81.15.4917.

78. Atzeni, F., Schena, M., Ongari, A.M., Carrabba, M., Bonara, P., Minonzio, F., and Capsoni, F. (2002). Induction of CD69 activation molecule on human neutrophils by GM-CSF, IFN-gamma, and IFN-alpha. Cell.Immunol. *220*, 20–29. https://doi.org/10.1016/s0008-8749(03)00002-9.

79. Benet, Z., Jing, Z., and Fooksman, D.R. (2021). Plasma cell dynamics in the bone marrow niche. Cell Rep. *34*, 108733. https://doi.org/10.1016/j.celrep.2021.108733.

80. Ricker, E., Manni, M., Flores-Castro, D., Jenkins, D., Gupta, S., Rivera-Correa, J., Meng, W., Rosenfeld, A.M., Pannellini, T., Bachu, M., et al. (2021). Altered function and differentiation of age-associated B cells contribute to the female bias in lupus mice. Nat. Commun. *12*, 4813. https://doi.org/10.1038/s41467-021-25102-8.

81. Lightman, S.M., Utley, A., and Lee, K.P. (2019). Survival of long-lived plasma cells (LLPC): piecing together the puzzle. Front. Immunol. *10*, 965. https://doi.org/10.3389/fimmu.2019.00965.

82. Baran-Gale, J., Morgan, M.D., Maio, S., Dhalla, F., Calvo-Asensio, I., Deadman, M.E., Handel, A.E., Maynard, A., Chen, S., Green, F., et al. (2020). Ageing compromises mouse thymus function and remodels epithelial cell differentiation. Elife *9*, e56221. https://doi.org/10.7554/eLife.56221.

83. Tomay, F., Wells, K., Duong, L., Tsu, J.W., Dye, D.E., Radley-Crabb, H.G., Grounds, M.D., Shavlakadze, T., Metharom, P., Nelson, D.J., and Jackaman, C. (2018). Aged neutrophils accumulate in lymphoid tissues from healthy elderly mice and infiltrate T- and B-cell zones. Immunol. Cell Biol. *96*,

831–840. https://doi.org/10.1111/imcb.12046.

84. Kuley, R., Draves, K.E., Fuller, D.H., Giltiay, N.V., Clark, E.A., and Giordano, D. (2021). B cell activating factor (BAFF) from neutrophils and dendritic cells is required for protective B cell responses against Salmonella typhimurium infection. PLoS One *16*, e0259158. https://doi.org/10.1371/journal.pone.0259158.

85. Parsa, R., Lund, H., Georgoudaki, A.M., Zhang, X.M., Ortlieb Guerreiro-Cacais, A., Grommisch, D., Warnecke, A., Croxford, A.L., Jagodic, M., Becher, B., et al. (2016). BAFF-secreting neutrophils drive plasma cell responses during emergency granulopoiesis. J. Exp. Med. *213*, 1537–1553. https://doi.org/10.1084/jem.20150577.

86. Wilhelmson, A.S., Lantero Rodriguez, M., Stubelius, A., Fogelstrand, P., Johansson, I., Buechler, M.B., Lianoglou, S., Kapoor, V.N., Johansson, M.E., Fagman, J.B., et al. (2018). Testosterone is an endogenous regulator of BAFF and splenic B cell number. Nat. Commun. *9*, 2067. https://doi.org/10.1038/s41467-018-04408-0.

87. Walters, S.N., Webster, K.E., Daley, S., and Grey, S.T. (2014). A role for intrathymic B cells in the generation of natural regulatory T cells. J. Immunol. *193*, 170–176. https://doi.org/10.4049/jimmunol.1302519.

88. Inaba, M., Inaba, K., Adachi, Y., Nango, K., Ogata, H., Muramatsu, S., and Ikehara, S. (1990). Functional analyses of thymic CD5+ B cells. Responsiveness to major histocompatibility complex class II-restricted T blasts but not to lipopolysaccharide or anti-IgM plus interleukin 4. J. Exp. Med. *171*, 321–326. https://doi.org/10.1084/jem.171.1.321.

89. Inaba, M., Inaba, K., Fukuba, Y., Mori, S., Haruna, H., Doi, H., Adachi, Y., Iwai, H., Hosaka, N., Hisha, H., et al. (1995). Activation of thymic B cells by signals of CD40 molecules plus interleukin-10. Eur. J. Immunol. *25*, 1244–1248. https://doi.org/10.1002/eji.1830250517.

90. Foss, D.L., Donskoy, E., and Goldschneider, I. (2001). The importation of hematogenous precursors by the thymus is a gated phenomenon in normal adult mice. J. Exp. Med. *193*, 365–374. https://doi.org/10.1084/jem.193.3.365.

91. Price, M.J., Hicks, S.L., Bradley, J.E., Randall, T.D., Boss, J.M., and Scharer, C.D. (2019). IgM, IgG, and IgA influenza-specific plasma cells express divergent transcriptomes. J. Immunol. *203*, 2121–2129. https://doi.org/10.4049/jimmunol.1900285.

92. Wilmore, J.R., Gaudette, B.T., Gómez Atria, D., Rosenthal, R.L., Reiser, S.K., Meng, W., Rosenfeld, A.M., Luning Prak, E.T., and Allman, D. (2021). IgA plasma cells are long-lived residents of gut and bone marrow that express isotype- and tissue-specific gene expression patterns. Front. Immunol. *12*, 791095. https://doi.org/10.3389/fimmu.2021.791095.

93. Neumeier, D., Pedrioli, A., Genovese, A., Sandu, I., Ehling, R., Hong, K.L., Papadopoulou, C., Agrafiotis, A., Kuhn, R., Shlesinger, D., et al. (2022). Profiling the specificity of clonally expanded plasma cells during chronic viral infection by single-cell analysis. Eur. J. Immunol. *52*, 297–311. https://doi.org/10.1002/eji.202149331.

94. Yamano, T., Nedjic, J., Hinterberger, M., Steinert, M., Koser, S., Pinto, S., Gerdes, N., Lutgens, E., Ishimaru, N., Busslinger, M., et al. (2015). Thymic B cells are licensed to present self antigens for central T cell tolerance induction. Immunity *42*, 1048–1061. https://doi.org/10.1016/j.immuni.2015.05.013.

95. Dodd, K.C., and Menon, M. (2022). Sex bias in lymphocytes: implications for autoimmune diseases. Front. Immunol. *13*, 945762. https://doi.org/10.3389/fimmu.2022.945762.

96. Passos, V., Pires, A.R., Foxall, R.B., Nunes-Cabaço, H., and Sousa, A.E. (2022). Expression of human endogenous retroviruses in the human thymus along T cell development. Front. Virol. *2*, 8. https://doi.org/10.3389/fviro.2022.826393.

97. Colantonio, A.D., Epeldegui, M., Jesiak, M., Jachimowski, L., Blom, B., and Uittenbogaart, C.H. (2011). IFN-alpha is constitutively expressed in the human thymus, but not in peripheral lymphoid organs. PLoS One *6*, e24252. https://doi.org/10.1371/journal.pone.0024252.

98. Papalexi, E., and Satija, R. (2018). Single-cell RNA sequencing to explore immune cell heterogeneity. Nat. Rev. Immunol. *18*, 35–45. https://doi.org/10.1038/nri.2017.76.

99. Lun, A.T.L., Riesenfeld, S., Andrews, T., Dao, T.P., Gomes, T.; participants in the 1st Human Cell Atlas Jamboree, and Marioni, J.C. (2019). EmptyDrops: distinguishing cells from empty droplets in droplet-based single-cell RNA sequencing data. Genome Biol. *20*, 63. https://doi.org/10.1186/s13059-019-1662-y.

100. Amezquita, R.A., Lun, A.T.L., Becht, E., Carey, V.J., Carpp, L.N., Geistlinger, L., Marini, F., Rue-Albrecht, K., Risso, D., Soneson, C., et al. (2020). Orchestrating single-cell analysis with Bioconductor. Nat. Methods *17*, 137–145. https://doi.org/10.1038/s41592-019-0654-x.

101. McCarthy, D.J., Campbell, K.R., Lun, A.T.L., and Wills, Q.F. (2017). Scater: pre-processing, quality control, normalization and visualization of single-cell RNA-seq data in R. Bioinformatics *33*, 1179–1186. https://doi.org/10.1093/bioinformatics/btw777.

102. Stuart, T., Butler, A., Hoffman, P., Hafemeister, C., Papalexi, E., Mauck, W.M., 3rd, Hao, Y., Stoeckius, M., Smibert, P., and Satija, R. (2019). Comprehensive integration of single-cell data. Cell *177*, 1888–1902.e21. https://doi.org/10.1016/j.cell.2019.05.031.

103. Bunis, D.G., Andrews, J., Fragiadakis, G.K., Burt, T.D., and Sirota, M. (2020). dittoSeq: universal user-friendly single-cell and bulk RNA sequencing visualization toolkit. Bioinformatics *36*, 5535–5536. https://doi.org/10.1093/bioinformatics/btaa1011.

104. Street, K., Risso, D., Fletcher, R.B., Das, D., Ngai, J., Yosef, N., Purdom, E., and Dudoit, S. (2018). Slingshot: cell lineage and pseudotime inference for single-cell transcriptomics. BMC Genom. *19*, 477. https://doi.org/10.1186/s12864-018-4772-0.

105. Ilicic, T., Kim, J.K., Kolodziejczyk, A.A., Bagger, F.O., McCarthy, D.J., Marioni, J.C., and Teichmann, S.A. (2016). Classification of low quality cells from single-cell RNA-seq data. Genome Biol. *17*, 29. https://doi.org/10.1186/s13059-016-0888-1.

STAR★METHODS

KEY RESOURCES TABLE

REAGENT or RESOURCE	SOURCE	IDENTIFIER
Antibodies		
CD138-BV421 (Clone: 281-2)	BD Biosciences	Cat# 562610; RRID: AB_11153126
IgD-BV605 (Clone: 11-26c.2a)	BioLegend	Cat# 405727; RRID: AB_2562887
IgD-APC (Clone: 11-6c.2a)	BioLegend	Cat# 405714; RRID: AB_10643423
CD90.2(Thy-1.2)-BV605 (Clone: 53-2.1)	BD Biosciences	Cat# 563008; RRID: AB_2665477
CD90.2(Thy-1.2)-APC (Clone: 53-2.1)	BD Biosciences	Cat# 553007; RRID: AB_398526
CD45R(B220)-PerCP/Cy5.5 (Clone: RA3-6B2)	BD Biosciences	Cat# 552771; RRID: AB_394457
CD45R(B220)-BV711 (Clone: RA3-6B2)	BD Biosciences	Cat# 563892; RRID: AB_2738470
CD19-BUV395 (Clone: 1D3)	BD Biosciences	Cat# 563557; RRID: AB_2722495
CD19-PE (Clone: 1D3)	BioLegend	Cat# 152408; RRID: AB_2629817
CD19-eFluor 450 (Clone: eBio1D3)	Thermo Fisher Scientific	Cat# 48-0193-82; RRID: AB_2734905
TCRβ-BV605 (Clone: H57-597)	BioLegend	Cat# 109241; RRID: AB_2629563
CD16/32-Unlabeled (Clone: 93)	Thermo Fisher Scientific	Cat# 14-0161-86; RRID: AB_467135
CD44-PE/Cy7 (Clone: IM7)	Thermo Fisher Scientific	Cat# 25-0441-81; RRID: AB_469622
CD267(TACI)-PE (Clone: 8F10)	BioLegend	Cat# 133403; RRID: AB_2203542
CD267(TACI)-AF647 (Clone: 8F10)	BD Biosciences	Cat# 558453; RRID: AB_647119
GL7-AF647 (Clone: GL7)	BD Biosciences	Cat# 561529; RRID: AB_10716056
CD95(Fas)-PE (Clone: Jo2)	BD Biosciences	Cat# 554258; RRID: AB_395330
CD69-PE/Cy7 (Clone: H1.2F3)	BD Biosciences	Cat# 561930; RRID: AB_10893591
I-A/I-E(MHC II)-AF647 (Clone: M5/114.15.2)	BioLegend	Cat# 107618; RRID: AB_493525
Ly-6C-PE (Clone: HK1.4)	BioLegend	Cat# 128008; RRID: AB_1186132
CD287(TLR7)-PE (Clone: A04B10)	BD Biosciences	Cat# 565557; RRID: AB_2739295
Mouse IgG1-PE isotype control (Clone: MOPC-21)	BD Biosciences	Cat# 554680; RRID: AB_395506
CD45-PE (Clone: 30F11)	BioLegend	Cat# 103106; RRID: AB_312971
CD45-APC (Clone: 30F11)	BioLegend	Cat# 103112; RRID: AB_312977
Igκ-PE (Clone: RMK-45)	BioLegend	Cat# 409505; RRID: AB_2563580
Igκ-FITC (Clone: RMK-45)	BioLegend	Cat# 409510; RRID: AB_2563585
Igλ-PE (Clone: RML-42)	BioLegend	Cat# 407308; RRID: AB_1027659
Igλ-FITC (Clone: R26-46)	BD Biosciences	Cat# 553434; RRID: AB_394854
Ly-6A/E(Sca-1)-PE/Cy7 (Clone: D7)	BioLegend	Cat# 108113; RRID: AB_493597
CD184(CXCR4)-APC (Clone: L276F12)	BioLegend	Cat# 146507; RRID: AB_2562784
Mouse IgG2b-FITC isotype control (Clone: RTK4530)	BioLegend	Cat# 400606; RRID: AB_326550
Ki-67-FITC (Clone: 11F6)	BioLegend	Cat# 151212; RRID: AB_2814055
Rat IgG2a-FITC isotype control (Clone: RTK2758)	BioLegend	Cat# 400506; RRID: AB_2736919
CD40-FITC (Clone: 3/23)	BioLegend	Cat# 124608; RRID: AB_1134096
Mouse IgG-Unlabeled	SouthernBiotech	Cat# 0107-01; RRID: AB_2732898
Anti-mouse IgG+IgA+IgM (H+L)	Millipore Sigma	Cat# SAB3701043-2MG
Goat anti-mouse IgM-HRP	Thermo Fisher Scientific	Cat# 62-6820; RRID: AB_2533954
Goat anti-mouse IgG-HRP	SouthernBiotech	Cat# 1015-05; RRID: AB_2794194
InVivoMab polyclonal Armenian hamster IgG isotype control	Bio X Cell	Cat# BE0091; RRID: AB_1107773

(*Continued on next page*)

Continued

REAGENT or RESOURCE	SOURCE	IDENTIFIER
InVivoMab anti-mouse CD154(CD40L) (Clone: MR-1)	Bio X Cell	Cat# BE0017-1; RRID: AB_1107601
InVivoMab rat IgG2a isotype control (Clone: 2A3)	Bio X Cell	Cat# BE0089; RRID: AB_1107769
InVivoMab anti-mouse CD40 (Clone: FGK4.5/FGK45)	Bio X Cell	Cat# BE0016-2; RRID: AB_1107647
Chemicals, peptides, and recombinant proteins		
InVivoPure pH 7.0 Dilution Buffer	Bio X Cell	Cat# IP0070
Bovine Serum Albumin (DNase- and Protease-free)	Fisher Scientific	Cat# BP9706100
APRIL	Fisher Scientific	Cat# 7907-AP-010CF
IL-6	Fisher Scientific	Cat# PMC0066
Critical commercial assays		
Platinum II Host-Start PCR Master Mix (2x)	Thermo Fisher Scientific	Cat# 14000012
Chromium Next GEM Single Cell 5′ Library and Gel Bead Kit v1.1	10x Genomics	Cat# 1000165
Chromium Next GEM Chip G Single Cell Kit	10x Genomics	Cat# 1000120
Chromium Single Cell V(D)J Enrichment Kit, Mouse B Cell	10x Genomics	Cat# 1000072
Chromium i7 Multiplex Kit	10x Genomics	Cat# 120262
Beckman Coulter SPRIselect	Fisher Scientific	Cat# NC0406406
Dynabeads MyOne Silane	Thermo Fisher Scientific	Cat# 37002D
Collibri Library Quantification Kit	Thermo Fisher Scientific	Cat# A38524500
High Sensitivity DNA Kit	Agilent	Cat# 5067-4626
AEC Substrate Set	BD Biosciences	Cat# 551951; RRID: AB_2868954
eBioscience Fixable Viability (Live-Dead) Dye eFluor 780	Thermo Fisher Scientific	Cat# 65-0865-14
Foxp3/Transcription Factor Staining Buffer Set	Thermo Fisher Scientific	Cat# 00-5523-00
Deposited data		
ASC scRNA-Seq GEX and VDJ data	This paper	GEO: GSE193701
Original code related to scRNA-Seq analysis	This paper	https://github.com/vari-bbc/Pioli_2022_ASCs_code
Experimental models: Organisms/strains		
Mouse: C57BL/6J	The Jackson Laboratory	JAX: 000664; RRID: IMSR_JAX:000664
Mouse: B6.Cg-Tg(Prdm1-EYFP)1Mnz/J	The Jackson Laboratory	JAX: 008828; RRID: IMSR_JAX:008828
Mouse: B6.129-*Prdm1*$^{tm1Clme/}$J	The Jackson Laboratory	JAX: 008100; RRID: IMSR_JAX:008100
Mouse: B6.C(Cg)-*Cd79a*$^{tm1(cre)Reth/}$EhobJ	The Jackson Laboratory	JAX: 020505; RRID: IMSR_JAX:020505
Oligonucleotides		
Prdm1-eYFP Genotyping Forward Primer: TTCCACAGCTCTGAGGGTCT	The Jackson Laboratory	https://www.jax.org/Protocol?stockNumber=008828&protocolID=25522
Prdm1-eYFP Genotyping Reverse Primer: CGGTGGTGCAGATGAACTT	The Jackson Laboratory	https://www.jax.org/Protocol?stockNumber=008828&protocolID=25522
Prdm1 Floxed Genotyping Forward Primer: CAATGCTTGTCTAGTGTC	The Jackson Laboratory	https://www.jax.org/Protocol?stockNumber=008100&protocolID=22773
Prdm1 Floxed Genotyping Reverse Primer: AGTAGTTGAATGGGAGC	The Jackson Laboratory	https://www.jax.org/Protocol?stockNumber=008100&protocolID=22773
Mb1 (Cd79a) Genotyping Wildtype Forward Primer: CTCTTTACCTTCCAAGCACTGA	The Jackson Laboratory	https://www.jax.org/Protocol?stockNumber=029412&protocolID=20206
Mb1 (Cd79a) Genotyping Common Reverse Primer: ACTGAGGCAGGAGGATTGG	The Jackson Laboratory	https://www.jax.org/Protocol?stockNumber=029412&protocolID=20206

(*Continued on next page*)

Continued

REAGENT or RESOURCE	SOURCE	IDENTIFIER
Mb1 (Cd79a) Genotyping Mutant Forward Primer: CATTTTCGAGGGAGCTTCA	The Jackson Laboratory	https://www.jax.org/Protocol?stockNumber=029412&protocolID=20206
Software and algorithms		
FlowJo (v10)	BD Biosciences	RRID: SCR_008520
GraphPad Prism 8	GraphPad Software	RRID: SCR_002798
Adobe Illustrator	Adobe	RRID: SCR_010279
Adobe Photoshop	Adobe	RRID: SCR_014199
Cell Ranger v6.0	10x Genomics	https://support.10xgenomics.com/single-cell-gene-expression/software/downloads/latest
DropletUtils v1.12.2	Lun et al.[99]	https://bioconductor.org/packages/release/bioc/html/DropletUtils.html
scuttle v1.2.0	Amezquita et al.[100]; McCarthy et al.[101]	https://bioconductor.org/packages/release/bioc/html/scuttle.html
Seurat v4.0.3	Stuart et al.[102]	https://satijalab.org/seurat/
dittoSeq v1.4.1	Bunis et al.[103]	https://bioconductor.org/packages/devel/bioc/vignettes/dittoSeq/inst/doc/dittoSeq.html
scran v1.20.1	Lun et al., 2016	https://bioconductor.org/packages/release/bioc/html/scran.html
Slingshot v2.0.0	Street et al.[104]	https://bioconductor.org/packages/release/bioc/html/slingshot.html
tradeSeq v1.6.0	Van den Berge et al.[58]	https://www.bioconductor.org/packages/release/bioc/html/tradeSeq.html
scRepertoire v1.3.5	Borcherding et al.[69]	http://www.bioconductor.org/packages/release/bioc/vignettes/scRepertoire/inst/doc/vignette.html

RESOURCE AVAILABILITY

Lead contact

Further information and requests for resources and reagents should be directed to and will be fulfilled by the lead contact, Peter Dion Pioli (peter.pioli@usask.ca).

Materials availability

Materials underlying this article will be shared by the lead contact upon request.

Data and code availability

- Single cell RNA-sequencing data have been deposited in the NCBI Gene Expression Omnibus (GEO) database and is accessible under accession number GSE193701 which is listed in the key resources table. Flow cytometry data reported in this study will be shared by the lead contact upon request.
- All original code is publicly available at https://github.com/vari-bbc/Pioli_2022_ASCs_code.
- Any information required for data reanalysis is available from the lead contact upon request.

EXPERIMENTAL MODEL AND SUBJECT DETAILS

Experimental animals

Mouse strains C57BL/6J (Stock #: 000664), B6.Cg-Tg(Prdm1-EYFP)1Mnz/J (Stock #: 008828), B6.129-*Prdm1*^{tm1Clme}/J (Stock #: 008100) and B6.C(Cg)-*Cd79a*$^{tm1(cre)Reth}$/EhobJ (Stock #: 020505) were purchased from The Jackson Laboratory. Mice were considered young at 3-5 mo.of age. Mice were considered middle-aged at 12 mo.of age. Female and male mice were utilized for all experiments. Animal care and use

were conducted according to the guidelines of the Western Michigan University Homer Stryker M.D. School of Medicine (WMed) Institutional Animal Care and Use Committee (IACUC) as well as the University of Saskatchewan (USask) University Animal Care Committee (UACC) Animal Research Ethics Board. All animals were housed and/or bred in the WMed vivarium or the USask Lab Animals Services Unit.

METHOD DETAILS

Isolation of bone marrow, spleen and thymus tissue

All tissues were processed and collected in calcium and magnesium-free 1xphosphate buffered saline (PBS). Spleen (SPL) and thymus (THY) were dissected and crushed between the frosted ends of two slides. Bone marrow (BM) was isolated from both femurs and tibias by cutting off the end of bones and flushing the marrow from the shaft using a 23-gauge needle. Cell suspensions were centrifuged for 5 minutes at 4 °C and 600g. Red blood cells were lysed by suspending cells in 3 mL of 1x red blood cell lysis buffer on ice for ~3 minutes. Lysis was stopped with the addition of 7 mL of 1x PBS. Cell suspensions were counted in a hemocytometer using Trypan Blue to exclude dead cells and passed through 40-μm filters before use.

Whole blood was obtained via cardiac puncture and immediately transferred to EDTA containing tubes on ice. 100 μL was directly mixed with 3 mL of 1x red blood cell lysis buffer and placed on ice for ~3 minutes. Lysis was stopped with the addition of 7 mL of 1x PBS.

Immunostaining

All staining procedures were performed in 1x PBS +0.1% bovine serum albumin (BSA). Samples were labeled with a CD16/32 blocking antibody (Ab) to eliminate non-specific binding of Abs to cells via Fc receptors. All Abs utilized are listed in the key resources table. For surface staining, cells were incubated on ice for 30 minutes with the appropriate Abs. Unbound Abs were washed from cells with 1x PBS +0.1% BSA followed by centrifugation for 5 minutes at 4 °C and 600g. Supernatants were decanted and cell pellets were resuspended in an appropriate volume of 1x PBS +0.4% BSA +2 mM EDTA for flow cytometric analysis. Before analysis, cells were strained through a 40 μM filter mesh.

Intracellular staining was performed using the Foxp3/Transcription Factor Staining Buffer Set. Cells were surface stained as described above. Afterwards, cell pellets were resuspended in 1 mL of buffer #1 and incubated at room temperature (RT) for 30 minutes in the dark. Subsequently, 2 mL of buffer #2 were added and cells centrifuged for 5 minutes at RT and 600g. Supernatants were discarded and cells were blocked with total mouse IgG at RT in the dark for 20-30 minutes. Cells were then incubated with either target specific or isotype control Abs. Following this incubation, 2 mL of buffer #2 were added and cells centrifuged for 5 minutes at RT and 600g. Finally, cells were washed with 3 mL of 1x PBS +0.1% BSA and centrifuged for 5 minutes at RT and 600g. Cells were prepped for flow cytometric analysis as described above. For all intracellular stains, eBioscience Fixable Viability (Live-Dead) Dye eFluor 780 (Thermo Fisher Scientific, Catalog # 65-0865-14) was added to samples to assess dead cell content. The stock solution was diluted 1:250 and 10 μL was added to ~5 x 10^6 cells per stain. Live-Dead stain was added concurrent with surface staining Abs.

Flow cytometry and fluorescence-activated cell sorting

Flow cytometry was performed on a Fortessa (BD Biosciences) located in the Flow Cytometry and Imaging Core at WMed. Total cells were gated using side scatter area (SSC-A) versus forward scatter (FSC-A) area. Singlets were identified using sequential gating of FSC-width (W) versus FSC-A, SSC-W versus SSC-A and FSC-height (H) versus FSC-A. Additional flow cytometry experiments were performed on a CytoFLEX (Beckman Coulter) located in the Cancer Cluster at USask. Total cells were gated using side scatter area (SSC-A) versus forward scatter (FSC-A) area. Singlets were identified using sequential gating of SSC-H versus SSC-A and FSC-H versus FSC-A. All data were analyzed using FlowJo (v10) software.

Fluorescence-activated cell sorting (FACS) was performed on a Melody (BD Biosciences) located in the Flow Cytometry and Imaging Core at WMed. Prior to sorting, cells were resuspended at a final concentration of 2x10^7 cells per mL in αMEM supplemented with HEPES (25 mM), Penicillin-Streptomycin (100 U/mL), L-glutamine (2 mM), Gentamicin (50 μg/mL) and EDTA (2 mM) and subsequently passed through a 40 μM filter mesh. Total cells were gated using SSC-A versus FSC-A. Singlets were identified using sequential gating of FSC-W versus FSC-A, SSC-W versus SSC-A and FSC-H versus FSC-A.

Enzyme-linked immunosorbent spot assay

Enzyme-linked immunosorbent spot (ELISpot) plates (Millipore Sigma, Cat# MSIPS4W10) were briefly incubated at RT for 1 minute with 15 μL of 35% ethanol (EtOH). EtOH was removed and wells were washed 3 times with 150 μL of 1x PBS. Subsequently, wells were coated overnight (O/N) at 4 °C with 100 μL of capture Ab. The capture Ab (Millipore Sigma, Cat# SAB3701043-2MG) recognized mouse total IgG+IgM+IgA isotypes and was pre-diluted in 1x PBS to a final concentration of 5 μg/mL before use. The next day, coating Abs were removed and wells were washed 3 times with 150 μL RPMI 1640. Plates were subsequently blocked with 150 μL RPMI for a minimum of 2 hours at 37 °C in a 5% CO_2/20% O_2 tissue culture incubator. Blocking solution was removed and 100 μL of RPMI supplemented with a proliferation-inducing ligand (APRIL) (10 ng/mL), interleukin (IL)-6 (10 ng/mL), heat-inactivated fetal calf serum (10%), Penicillin-Streptomycin (100 U/mL), L-glutamine (2 mM), Gentamicin (50 μg/mL), sodium pyruvate (1 mM), non-essential amino acids (1x), non-essential vitamins (1x) and 2-mercaptoethanol (10^{-05} M). ASCs from BM, SPL and THY were directly FACS-purified into wells with a target number of 100 cells per well. Cells were then incubated O/N (>12 hours) at 37 °C in a 5% CO_2/20% O_2 tissue culture incubator. The next day, culture supernatants and cells were removed. Wells were washed 3 times with 150 μL of 1x PBS then an additional 3 times with 150 μL of 1x PBS +0.1% Tween-20 + 1% BSA. Secondary Abs conjugated to horseradish peroxidase (HRP) were added at a volume of 100 μL per well and plates were incubated for 2 hours at RT. Anti-IgM-HRP (Thermo Fisher Scientific, Cat# 62-6820) and anti-IgG-HRP (SouthernBiotech, Cat# 1015-05) were diluted 1:25,000 and 1:50,000 in 1x PBS +0.1% Tween-20 + 1% BSA before use, respectively. Following incubation, Abs were removed plates washed 3 times with 150 μL of 1x PBS +0.1% Tween-20 + 1% BSA. An additional 3 washes with 150 μL of 1x PBS were performed. To reveal "spots", 100 μL of Developing Solution from the AEC Substrate Set (BD Biosciences, Cat# 551951) was added to each well. Plates were shaken at 200 rpm for 30 minutes at RT. Developing Solution was removed and plates were washed 5 times with 150 μL of H_2O. Well backing was removed and plates were dried at RT after which "spots" were visualized with a CTL ELISPOT reader. Additional wells lacking capture Abs or the use of secondary detection reagents were developed to gauge background. Using Adobe Photoshop, auto-contrast was uniformly applied to wells and brightness was set to 100 for visualization.

In vivo CD45 labeling

Young (3-4 mo.old) mice received either 1x PBS or αCD45-PE (1 μg) antibody in a 100 μL volume via intravenous (i.v.) injection into the retro-orbital (r.o.) sinus. Mice were euthanized 5 minutes or 24 hours post-injection for analysis.

*In vivo*CD154(CD40L) blockade

Young (3-5 mo.old) mice received a total of 600 μg or 1200 μg of hamster IgG isotype control or anti-mouse CD154(CD40L) (MR-1) antibodies. Administration was split evenly amongst 6 or 12 total intraperitoneal (i.p.) injections (100 μg per injection, 100 μl volume) over a 2-week or 4-week span after which mice were euthanized for analysis. Antibodies were supplied by Bio X Cell and pre-diluted to 1000 μg/mL using InVivoPure pH 7.0 Dilution Buffer.

In vivo CD40 stimulation

On days -1 and 0, young (3-4 mo.old) mice were administered 100 μg (100 μl volume) of rat IgG2a isotype control or agonistic anti-mouse CD40 antibodies per injection via the i.p. route. Antibodies were supplied by Bio X Cell and pre-diluted to 1000 μg/mL using InVivoPure pH 7.0 Dilution Buffer. Mice were euthanized for analysis on days 2, 4, 6 and 28 following the last injection.

10x genomics single cell library preparation, sequencing and analysis

ASCs from BM, SPL and THY were FACS-purified and collected into 1x PBS +0.1% BSA. Recovery was verified by hemocytometer count and/or analysis via flow cytometry. Cells were concentrated in a volume of 40 μL following centrifugation for 10 minutes at 4 °C and 600g. A volume of 37.8 μL of cells was loaded into a Chromium Next GEM Chip G and single cell gel emulsions were generated on a 10x Genomics Chromium Controller. 10x Genomics barcoded full-length cDNA was then synthesized on a Veriti 96-Well Thermal Cycler (Thermo Fisher Scientific) using the standard 10x Genomics protocol. Following initial recovery and cleanup, cDNA was amplified 18 cycles based upon manufacturer recommendations.

V(D)J-enriched libraries and gene expression (GEX) libraries were generated using the Chromium Single Cell V(D)J Enrichment Kit, Mouse B Cell (10x Genomics, Cat# 1000072) and Chromium Next GEM Single Cell 5' Library and Gel Bead Kit v1.1 (10x Genomics, Cat# 1000165), respectively. All libraries were sample indexed for multiplexing with the Chromium i7 Multiplex Kit (10x Genomics, Cat# 120262) following standard 10x Genomics protocols. All completed libraries were visualized and quantified using an Agilent 2100 Bioanalyzer. Furthermore, qPCR utilizing the Collibri Library Quantification Kit (Thermo Fisher Scientific, Cat# A38524500) was performed to verify the suitability of each library for sequencing. V(D)J libraries were pooled in tandem based upon organ and population (e.g., Female and Male THY ASC) and sequenced on an Illumina MiSeq inhouse. All 6 GEX libraries were pooled and sequenced simultaneously on a NovaSeq 6000 at the Van Andel Institute Genomics Core.

Reads were aligned to the mm10 reference genome ('refdata-gex-mm10-2020-A' provided by 10x) to obtain unique molecular identifier (UMI) counts using the cellranger count pipeline v6.0.2 with default parameters. The filtered counts matrices, with non-cell-associated barcodes removed, were imported into R v4.1.0 as a SingleCellExperiment object using DropletUtils v1.12.2.[99] Low total UMI counts or number of genes detected indicate low-quality cells while a high percent of reads mapping to mitochondrial genes suggest lysed cells.[105] To filter by these metrics, median absolute deviations (MAD) for these metrics were calculated for each sample separately and 3 MAD from the median was used as a cutoff, as implemented in the 'perCellQCMetrics' and 'quickPerCellQC' functions in the scuttle package v1.2.0.[100,101] A total of 3122 cells, with 1359 from the female bone marrow sample, were removed due to high mitochondrial gene expression but none were removed based on the other two metrics.

The filtered SingleCellExperiment object was converted to a Seurat (v4.0.3) object for 'integration' (batch correction) across the samples and for cluster identification using the standard Seurat integration workflow.[102] Briefly, the Seurat object was split based on the sample. UMI counts were normalized for total expression in each cell and log-transformed. The top 2000 most variable genes within each sample were identified, from which the 'anchor' genes for integration were chosen using the 'SelectIntegrationFeatures' function. The 'FindIntegrationAnchors' and 'IntegrateData' functions were used to perform batch correction using a method that utilizes mutual nearest neighbors (MNN) to identify biologically correspondent cells between datasets.[102] The corrected expression values were scaled and used for Principal Component Analysis (PCA). The top 30 principal components (PComs) were chosen for downstream analyses based on an elbow plot. For visualization, Uniform Manifold Approximation and Projection (UMAP) was performed on the top 30 PComs. Similarly, a shared nearest neighbor graph of the cells was constructed using the top 30 PComs and used for unsupervised clustering using the Louvain algorithm. Clustering was done at multiple resolutions ranging from 0.1 to 0.9, but the 0.3 resolution clustering was chosen for subsequent analyses. Various UMAP plots and bar charts were plotted using the dittoSeq v1.4.1 package.[103]

Marker genes for clusters were identified using the 'findMarkers' function in scran v1.20.1 with the parameters, 'pval.type="any"', 'direction="up"', 'test.type="wilcox"', 'min.prop=0.75' and setting block to the sample. This performs pairwise comparisons of each cluster to every other cluster, testing for up-regulation using Wilcoxon rank sum tests in each sample (i.e., block) separately; the p-values for each gene across all block levels are combined using Stouffer's Z-score method and the reported area under the curve (AUC) is a weighted average of the AUCs across all the block levels. For each gene and cluster, the summary effect size is the effect size from the pairwise comparison with the lowest p-value and the combined p-value is computed using Simes' method. The 'min.prop' parameter affects only the 'Top' column in the results. With 'min.prop' set to 0.75, genes with Top <= N are top N marker genes in at least 0.75 of the comparisons. Differentially expressed genes between samples within each cluster were identified using the 'FindMarkers' function in Seurat with 'logfc.threshold' set to 0.5. Only comparisons where both groups had greater than 20 cells were tested.

Pseudotime trajectories were inferred on the UMAP embedding using the 'slingshot' function in the Slingshot v2.0.0 package,[104] with the parameter 'approx_points=150' and setting the root at cluster 11, which had high expression of proliferative marker genes. To test for genes associated with pseudotime, the tradeSeq v1.6.0 package[58] was used. For genes with a count of at least 3 in at least 100 cells, a negative binomial generalized additive model (GAM) was fitted using the 'fitGAM' function, providing the batches (i.e., sample) using the 'U' argument. Pseudotime-associated genes were identified using the 'associationTest' function. Smoothed expression along pseudotime was plotted for various genes using the functions 'predictSmooth' and 'plotSmoothers'.

For VDJ analysis, reads were aligned to the mm10 VDJ reference provided by 10x ('refdata-cellranger-vdj-GRCm38-alts-ensembl-5.0.0') and assembled into contigs using the cellranger vdj pipeline v6.0.2 with default parameters. The 'filtered_contig_annotations.csv' files were read into R and combined for use with the scRepertoire v1.3.5 R package[69] using the 'combineBCR' function. Clonotype information was merged with the Seurat object using the 'combineExpression' function; this also calculated clonotype frequencies within each sample. Overlap of clonotypes was assessed by the Jaccard index using the 'clonalOverlap' function with the parameters, 'cloneCall="gene+nt"' and 'method="jaccard"'. IgH constant region gene expression was visualized using the 'vizGenes' function with the following parameters, 'gene="C"' and 'chain="IGH"'.

Code is available at: https://github.com/vari-bbc/Pioli_2022_ASCs_code. Sequencing data has been deposited in the NCBI Gene Expression Omnibus (GEO) database and is accessible under accession number GSE193701.

QUANTIFICATION AND STATISTICAL ANALYSIS

The numbers of mice used (n =) or replicates performed per experiment are listed in the Figure Legends. For non-genomics data, statistical analyses were performed using GraphPad Prism (v8.4.2) software. Quantification of cell numbers and various flow cytometry data are graphically represented as mean ± SEM. A Student's t-Test was used for statistical comparisons between 2 groups. For comparisons among 3 or more groups, a one-way ANOVA with Tukey's or Dunnett's correction was utilized. Both paired and unpaired tests were utilized where appropriate. Statistically significant p-values are shown within each figure.